NASA TECHNICAL NOTE

NASA TN D-7231

NASA TN D-7231

THE EFFECTS OF AN AUTOPILOT ON AIRPLANE RESPONSES TO TURBULENCE WITH EMPHASIS ON TAIL LOADS

by Boyd Perry III

Langley Research Center
Hampton, Va. 23665

NATIONAL AERONAUTICS AND SPACE ADMINISTRATION • WASHINGTON, D. C. • DECEMBER 1973

1. Report No.	2. Government Accession No.	3. Recipient's Catalog No.
NASA TN D-7231		

4. Title and Subtitle	5. Report Date
THE EFFECTS OF AN AUTOPILOT ON AIRPLANE RESPONSES TO TURBULENCE WITH EMPHASIS ON TAIL LOADS	December 1973
	6. Performing Organization Code

7. Author(s)	8. Performing Organization Report No.
Boyd Perry III	L-8756
	10. Work Unit No.
9. Performing Organization Name and Address	501-22-05-03
NASA Langley Research Center Hampton, Va. 23665	11. Contract or Grant No.
	13. Type of Report and Period Covered
12. Sponsoring Agency Name and Address	Technical Note
National Aeronautics and Space Administration Washington, D.C. 20546	14. Sponsoring Agency Code

15. Supplementary Notes

16. Abstract

An analytical study has been made to assess the loads developed on the horizontal tail of an autopilot-controlled rigid airplane flying in one-dimensional atmospheric turbulence. The root-mean-square values of rigid-airframe responses and tail-load responses were calculated at five flight conditions, and the behavior of these responses was observed in two autopilot modes: pitch-attitude-hold mode and altitude-control mode. It was found that pitch attitude and altitude can be controlled by the simple autopilot with acceptable or no increases in tail loads.

17. Key Words (Suggested by Author(s))	18. Distribution Statement
Atmospheric turbulence Autopilot Tail loads Airplane response	Unclassified – Unlimited

19. Security Classif. (of this report)	20. Security Classif. (of this page)	21. No. of Pages	22. Price*
Unclassified	Unclassified	55 ~~52~~	Domestic, $3.50 Foreign, $6.00

*For sale by the National Technical Information Service, Springfield, Virginia 22151

THE EFFECTS OF AN AUTOPILOT ON AIRPLANE RESPONSES TO TURBULENCE WITH EMPHASIS ON TAIL LOADS

By Boyd Perry III
Langley Research Center

SUMMARY

An analytical study has been made to assess the loads developed on the horizontal tail of an autopilot-controlled rigid airplane flying in one-dimensional atmospheric turbulence. The root-mean-square values of rigid-airframe responses and tail-load responses were calculated at five flight conditions, and the behavior of these responses was observed in two autopilot modes: pitch-attitude-hold mode and altitude-control mode. It was found that pitch attitude and altitude can be controlled by the simple autopilot with acceptable or no increases in tail loads.

INTRODUCTION

The functions of most autopilots in transport airplanes range from stabilizing motions that have poor or no inherent stability to maintaining the airplane on a prescribed flight path. In the process, the automatic-control system must compensate for changes in vehicle and flight conditions and for atmospheric disturbances. A number of studies have been conducted on the responses of autopilot-controlled airplanes to drafts and turbulence; however, these investigations were directed primarily toward responses in airplane motions and load factor (refs. 1 and 2). Presumably, designers' studies consider the tail loads associated with automatically controlled flight in turbulence, but practically no information appears in the literature on the subject.

An exploratory study, therefore, was made to reveal possible problem areas with regard to loads on the horizontal-tail surface arising from autopilot-controlled flight in turbulence. For this purpose, the airplane, autopilot, and turbulence are approximated by the simplest mathematical models that are felt to retain the elements which significantly influence the tail loads. The airplane is representative of the class of small corporate jet transports and is idealized as a rigid body in the longitudinal mode. The autopilot is approximated by the use of only first-order servosystem dynamics (ref. 3) and features pitch-attitude-hold and altitude-control modes through deflection of the elevator. The atmospheric turbulence is assumed to be one-dimensional for this analysis, and the usual assumptions of the characteristics for short Gaussian samples are made. The responses to turbulence include tail-load responses (in the form of root-mean-square values of shear

and bending moment at the root of the horizontal tail and torque about the horizontal-tail elastic axis) and airframe responses (root-mean-square values of pitch attitude, altitude perturbation, and center-of-gravity (c.g.) normal acceleration). In this study the various airframe and tail-load responses are calculated as functions of appropriate control-system gains for two centers of gravity, two cruise altitudes, and three autopilot servosystem lag conditions.

SYMBOLS

$a_{c.g.}$ normal acceleration of airplane center of gravity, positive up

a_t normal acceleration of horizontal tail, positive up

b_t span of horizontal tail

$C_{L,o}$ airplane lift coefficient at reference flight condition

$C_{L_{\alpha_t}}$ lift-curve slope of horizontal tail, $\partial C_{L_t} / \partial \alpha_t$

C_{L_t} lift coefficient of horizontal tail

$C_{L_{t_\delta}}$ elevator lift effectiveness, $\partial C_{L_t} / \partial \delta$

C_m pitching-moment coefficient

C_x longitudinal-force coefficient

C_z plunge-force coefficient

$\bar{c}$ mean aerodynamic chord of wing

$\bar{c}_t$ mean aerodynamic chord of horizontal tail

c_i effective moment-arm coefficient for force distribution $\ell_i(x)$ in appendix B

$c_t(y)$ chord of horizontal tail as function of span

c_1 effective moment-arm coefficient for additional lift distribution due to angle of attack

c_2 effective moment-arm coefficient for additional lift distribution due to elevator deflection

c_3 effective moment-arm coefficient for basic lift distribution due to elevator deflection

c_4 effective moment-arm coefficient for mass distribution

f frequency, hertz

f_o damped natural frequency, hertz

f_{w_g} matrix of vertical-gust forces

g acceleration due to gravity

$H_R(\omega)$ frequency-response function of response R

h altitude perturbation

h_{ref} desired altitude perturbation

I_{yy} mass moment of inertia about pitch axis

i_B nondimensional mass moment of inertia, $I_{yy} \Big/ \rho S \left(\frac{\bar{c}}{2}\right)^3$

K_h altitude-perturbation feedback gain

K_θ pitch-displacement feedback gain

$K_{\dot{\theta}}$ pitch-rate feedback gain

k_o damped natural reduced frequency, $\omega_o \bar{c} \Big/ 2u_o$

L scale of turbulence

L_{a_α} horizontal-tail additional lift due to angle of attack

L_{a_δ} horizontal-tail additional lift due to elevator deflection

L_{b_δ} horizontal-tail basic lift due to elevator deflection

L_t total lift on horizontal tail, $L_{a_\alpha} + L_{a_\delta} + L_{b_\delta}$

$\ell_{a_\alpha}(x)$ chordwise horizontal-tail additional-lift distribution due to angle of attack

$\ell_{a_\alpha}(y)$ spanwise horizontal-tail additional-lift distribution due to angle of attack

$\ell_{a_\delta}(x)$ chordwise horizontal-tail additional-lift distribution due to elevator deflection

$\ell_{a_\delta}(y)$ spanwise horizontal-tail additional-lift distribution due to elevator deflection

$\ell_{b_\delta}(x)$ chordwise horizontal-tail basic-lift distribution due to elevator deflection

$\ell_{b_\delta}(y)$ spanwise horizontal-tail basic-lift distribution due to elevator deflection

ℓ_h horizontal-tail length, distance from airplane center of gravity to horizontal-tail aerodynamic center

$\ell_i(x)$ general chordwise force distribution

$\ell_t(x)$ total chordwise horizontal-tail lift distribution

$\ell_t(y)$ total spanwise horizontal-tail lift distribution

M coefficient matrix of equations of motion

$M_b(\bar{y})$ horizontal-tail bending moment at spanwise location $\bar{y}$

m mass of airplane

$m_t(y)$ spanwise horizontal-tail mass distribution

q matrix of generalized coordinates in equations of motion

$\hat{q}$ nondimensional pitch rate

R general response to atmospheric turbulence

S wing area

S_t horizontal-tail area

s	Laplace variable
$T(\bar{y})$	torque about horizontal-tail elastic axis at spanwise location $\bar{y}$
t_{ch}	servosystem characteristic time
u	forward-speed perturbation
u_o	airplane forward speed
$\hat{u}$	nondimensional forward-speed perturbation, u/u_o
$V(\bar{y})$	horizontal-tail shear at spanwise location $\bar{y}$
w	perturbation velocity along z-axis, positive down
w_g	vertical gust velocity, positive up
x	chordwise coordinate
y	spanwise coordinate
$\bar{y}$	spanwise location
α	airplane angle-of-attack perturbation, w/u_o
α_g	gust angle of attack, w_g/u_o
α_t	horizontal-tail angle-of-attack perturbation (see appendix B)
α_w	wing angle-of-attack perturbation ($\alpha_w = \alpha$)
δ	elevator-deflection-angle perturbation, positive trailing edge down
ϵ	downwash angle at tail due to wing
ζ	damping ratio
θ	pitch-angle perturbation

θ_{ref} desired pitch-angle perturbation

λ_{EA} sweep angle of horizontal-tail elastic axis

$\lambda_{.25\bar{c}}$ sweep angle of wing quarter-chord

μ nondimensional mass, $m \Big/ \rho S \frac{\bar{c}}{2}$

ρ atmospheric mass density

σ_R root-mean-square value of response R

σ_{w_g} root-mean-square value of vertical gust velocity

τ transport time lag, ℓ_h / u_o

$\Phi_R(\omega)$ power spectrum for response R

$\Phi_{w_g}(\omega)$ power spectrum for vertical gust velocity

ϕ unsteady lift function

ω circular frequency, $2\pi f$

ω_o circular damped natural frequency, $2\pi f_o$

Nondimensional stability derivatives are indicated by subscript notation as follows:

$$C_{X_u} = \frac{\partial C_X}{\partial \hat{u}} \qquad C_{X_\alpha} = \frac{\partial C_X}{\partial \alpha}$$

$$C_{Z_u} = \frac{\partial C_Z}{\partial \hat{u}} \qquad C_{Z_\alpha} = \frac{\partial C_Z}{\partial \alpha} \qquad C_{Z_{\dot{\alpha}}} = \frac{\partial C_Z}{\partial \left(\frac{\dot{\alpha}\bar{c}}{2u_o} \right)}$$

$$C_{Z_{\hat{q}}} = \frac{\partial C_Z}{\partial \hat{q}}$$

$$C_{m_u} = \frac{\partial C_m}{\partial \hat{u}} \qquad C_{m_\alpha} = \frac{\partial C_m}{\partial \alpha} \qquad C_{m_{\dot{\alpha}}} = \frac{\partial C_m}{\partial \left(\frac{\dot{\alpha} \bar{c}}{2u_o} \right)}$$

$$C_{m_{\hat{q}}} = \frac{\partial C_m}{\partial \hat{q}}$$

$$C_{L_{\alpha_t}} = \frac{\partial C_{L_t}}{\partial \alpha_t} \qquad C_{L_{t_\delta}} = \frac{\partial C_{L_t}}{\partial \delta}$$

Subscripts:

$a_{c.g.}/g$	normal acceleration of airplane c.g.
a_t	normal acceleration of horizontal tail
EA	horizontal-tail elastic axis
h	altitude perturbation
L_{a_α}	horizontal-tail additional lift due to angle of attack
L_{a_δ}	horizontal-tail additional lift due to elevator deflection
L_{b_δ}	horizontal-tail basic lift due to elevator deflection
L_t	total lift on horizontal tail
M_b	horizontal-tail bending moment
T	horizontal-tail torque
$\hat{u}$	nondimensional forward speed perturbation
V	horizontal-tail shear
α	airplane angle-of-attack perturbation

α_t horizontal-tail angle-of-attack perturbation

δ elevator angle-of-attack perturbation

θ pitch-angle perturbation

METHOD OF ANALYSIS

Statistical Representation of Responses

The method for obtaining the airframe and tail-load responses to random atmospheric turbulence is explained herein. Random-process theory is a technique for statistically analyzing output or response data for linear systems. It relates the input (atmospheric disturbance) power spectral density function to the output (airframe and tail load) power spectral density functions through the various frequency-response functions (refs. 4 and 5). The power spectral density function (power spectrum) contains all the statistical information describing a Gaussian process, including the root-mean-square (rms) value.

The expression for the rms value of general response, R, per unit gust velocity is

$$\frac{\sigma_R}{\sigma_{w_g}} = \left[\frac{\int_0^\infty \Phi_R(\omega) d\omega}{\sigma_{w_g}^2} \right]^{1/2} \tag{1}$$

where σ_R is the rms value of response R (airframe response or tail-load response), σ_{w_g} is the rms value of the vertical component of gust velocity, and $\Phi_R(\omega)$ is the power spectral density function of response R. The upper limit of integration in equation (1) has a finite value in actual practice and is approximately equal to 200 radians per second. Also, for a linear system

$$\Phi_R(\omega) = \Phi_{w_g}(\omega) \left| H_R(\omega) \right|^2 \tag{2}$$

where $H_R(\omega)$ is the frequency-response function of response R to flight in a gust field which is sinusoidal in the direction of flight, has variable wavelengths, and is invariant in the spanwise direction. (See appendixes A and B for development of $H_R(\omega)$ from the equations of motion.) The Dryden representation of the one-dimensional atmospheric-turbulence power spectrum is given by

$$\Phi_{w_g}(\omega) = \frac{\sigma_{w_g}^2 L}{u_o \pi} \frac{1 + 3\frac{L^2}{u_o^2}\omega^2}{\left(1 + \frac{L^2}{u_o^2}\omega^2\right)^2} \tag{3}$$

The Dryden spectrum is chosen over the more accurate von Karman spectrum because of its simpler mathematical form; for the purposes of an exploratory study, the Dryden spectrum provides sufficient accuracy. For this study, the integral scale length L was chosen to be 762 m.

In conjunction with the equations of motion and the tail-load equations, which are discussed in appendixes A and B, equations (1), (2), and (3) are employed to obtain the rigid airframe and tail-load responses (in the form of rms values per unit rms gust velocity).

Mathematical Models

A rigid airplane, that is, one with rigid-airframe degrees of freedom but no elastic degrees of freedom, is assumed for this analysis. Its motion is described by the longitudinal degrees of freedom: forward speed, plunge, and pitch, featuring phugoid and short-period modes. The automatic-control system (autopilot) is idealized by assuming first-order servosystem dynamics. The idealized longitudinal autopilot consists of a pitch-attitude-hold mode and an altitude-control mode. Only one autopilot mode is operated at a time and no automatic trim device is considered. The equations of motion of the airplane autopilot system are basically the same as the classical equations of dynamic stability except that effects of the autopilot are included and appropriate gust forces are added. No unsteady-flow effects are included other than for transport time lags to account for the phase shift in the gust wave between wing and tail.

Figure 1 contains block diagrams of both autopilot modes. The attitude-hold autopilot is a pitch-displacement-type autopilot with a pitch-rate feedback loop for damping. Pitch-displacement feedback gain K_θ, and pitch-rate feedback gain $K_{\dot{\theta}}$, are the control-system gains. The altitude-control autopilot contains an altitude-perturbation feedback loop with control-system gain K_h (altitude-perturbation feedback gain). The "airplane-dynamics" boxes in the block diagrams contain the longitudinal equations of motion, and the "atmospheric-turbulence" boxes contain the gust forces. The "elevator-servo" boxes contain the transfer function describing the first-order servosystem dynamics. The mathematical description of these "boxes" is found in appendix A.

Tail Loads

The tail loads under investigation are shear and bending moment at the root of the horizontal tail and torque about the horizontal-tail elastic axis. The tail loads all consist of an aerodynamic component arising from airplane motions, gust velocities, and control deflections, and an inertial component arising from accelerations at the tail. Expressions for other responses, such as lift on the horizontal tail and accelerations at the tail (which are needed in defining tail loads), are listed in appendix B with the derivations of the tail-load equations.

AIRPLANE AND FLIGHT CONDITIONS

Airplane characteristics and flight conditions for this study are shown in tables I and II. Table I lists characteristics of the example airplane. The variations in cruise altitudes, centers-of-gravity, and servosystem dynamic conditions for each of the five flight conditions examined are listed in table II. Table III lists the airplane stability derivatives for each flight condition.

RESULTS AND DISCUSSION

Stability boundaries in terms of control-system gains and servosystem characteristic times, for both autopilot modes, are contained in table IV. The stability boundaries are determined by the familiar root-locus method, in which the exponentials describing the transport time lags are approximated by the first two terms of the exponential-series expansion. In the forced-response analysis, in which the transport time-lag exponentials are retained, the characteristic rapid increase in turbulence response with increasing autopilot gain identifies the approach of dynamic instability. The gains corresponding to the response peaks in the forced-response analysis are very nearly equal to the gains defining the stability boundaries determined by the root-locus method. Turbulence responses are obtained for only those combinations of gains and characteristic times which result in a stable airplane-autopilot configuration. The turbulence responses are found by employing equation (1) after the frequency responses for θ, h, $M_b(\bar{y})$, etc. have been obtained by solving the equations of motion and the tail-load equations.

Attitude-Hold Mode

The purpose of the attitude-hold autopilot is to maintain pitch attitude through pitch-displacement and pitch-rate feedback. The effects of varying K_θ and $K_{\dot{\theta}}$ on airframe and tail-load responses and additionally on the characteristic oscillatory motions are investigated for various flight conditions. The responses of interest in this autopilot mode are

pitch angle, c.g. normal acceleration, horizontal-tail bending moment, and horizontal-tail torque. Because of the similarity between the shear and bending-moment response curves, only bending-moment and torque response curves are presented. However, any discussion pertaining to bending moment also pertains to shear.

The characteristic motions for zero servosystem lag time are found to be stable for all values of displacement and rate gains. For small values of K_θ and $K_{\dot{\theta}}$ the characteristic motions consist of the oscillatory phugoid and short-period modes. As K_θ becomes large, the phugoid mode becomes overdamped ($\zeta > 1$) and transforms into two modes: one with a slowly decaying predominantly airspeed variation and the other with a rapidly decaying predominantly plunge motion. The short-period mode remains underdamped ($\zeta < 1$) but is transformed into a mode with a predominantly pitching motion as K_θ becomes large. The damped natural frequency of this pitching mode varies in proportion to $\sqrt{K_\theta}$ for large K_θ, as shown in figure 2.

The characteristic motions for nonzero servosystem lag times are not stable for all values of displacement and rate gains. The pitching mode becomes dynamically unstable at progressively lower values of displacement gain as the lag time is increased. The values of K_θ at instability are increased, however, by increasing the values of rate gain, as indicated in table IV.

Figures 3 to 7 contain plots of rms values of airframe responses (denoted by subscripts θ and $a_{c.g.}/g$) and tail-load responses (denoted by subscripts M_b and T) against displacement gain for the various flight conditions in the attitude-hold mode. The responses are plotted on the ordinate and the pitch-displacement feedback gain, K_θ, is plotted on the abscissa, which has a modified logarithmic scale broken near the left end to accommodate $K_\theta = 0$.

The five curves on each set of axes in figure 3 correspond to five values of rate gain, $K_{\dot{\theta}}$. The servosystem lag time equals zero for all curves. Pitch response decreases with increasing displacement gain, for all values of rate gain, because it is the controlled quantity. Large values of K_θ provide the smallest pitch response but the largest c.g. normal acceleration and tail-load responses. The c.g. normal-acceleration response increases and then approaches a constant value about 30 percent higher than that for the basic airplane as K_θ is increased. This trend reflects the loss of the airplane's natural tendency to pitch down into an up-gust as the pitching motion is suppressed. The c.g. normal-acceleration response at large K_θ is essentially that of an airplane restricted to plunging motion only. The tail-torque response exhibits a characteristic similar to the c.g. normal acceleration except that the increase is approximately doubled. Analysis of the torque-load components indicates that the aerodynamic torque load due to elevator deflection (for this particular combination of elevator-chord to horizontal-tail chord ratio and elastic-axis location) is small compared to the other load components. The torque

load at large values of K_θ is governed by the plunging motion as is the c.g. normal acceleration. The tail bending-moment response increases slowly for $K_\theta < 10$ and then rapidly thereafter. Analysis of the bending-moment load components indicates that the predominant contributor to bending moment is the elevator deflection. The rapid increase in the bending moment for $K_\theta > 10$ at smaller values of $K_{\dot{\theta}}$ is due to (1) a reduction in the pitching-mode damping ratio caused by the transport lag in downwash, and (2) a spatial resonance effect from the phase shift in the gust wave between wing and tail. For a sinusoidal gust field having a half wavelength equal to the distance between wing and tail, the pitching moments from the wing and tail are additive. This phenomenon results in a maximum pitching motion for airspeeds that cause this wavelength to coincide with the natural wavelength of the poorly damped oscillatory pitch mode. This condition occurs, for example, at a value of K_θ of about 300 and $K_{\dot{\theta}}$ of zero. Although not shown, the airspeed perturbation is not significantly excited by turbulence for $K_\theta = 0$ and the response decreases with increasing K_θ.

In general, the effect of adding rate feedback to the system is to increase the damping of the pitching motion and thus to reduce the magnitudes of all responses.

Effect of changing the airplane center-of-gravity location.- Figure 4 contains responses for flight conditions I and II. The effects of K_θ on airframe and tail-load responses for two c.g. locations at constant altitude are investigated. For the data presented in figure 4, $K_{\dot{\theta}}$ is held constant at a value of 10 and servosystem lag time is zero. As the c.g. is moved rearward (from $0.27\bar{c}$ to $0.31\bar{c}$), the short-period damping ratio increases and the damped natural frequency of the short period decreases. The former tends to reduce pitch response while the latter tends to increase pitch response. The effect of increased damping predominates, however, and there is a slight reduction in pitch response for all values of K_θ. The slight increase in c.g. normal-acceleration response occurs because the airframe's ability to "pitch into" gusts is reduced. The increase in bending-moment response with rearward c.g. shift is a result of the net increase in the aerodynamic component over the inertia component. The torque responses show that the rearward c.g. shift increases the torque about the tail elastic axis for small values of K_θ and decreases the torque for large values of $K_{\dot{\theta}}$.

Effect of changing cruise altitude.- Figure 5 contains responses for flight conditions I and III. The effects of K_θ on airframe and tail-load responses for two cruise altitudes at a specific center-of-gravity location are investigated. For the data presented in figure 5, $K_{\dot{\theta}}$ is again held constant at a value of 10 and servosystem lag time is again zero. There are significant changes in airframe and tail-load responses due to an increase in cruise altitude. Over the entire range of K_θ, reduced air density at the higher altitude results in an increased pitch response and a decreased c.g. normal-acceleration response.

Both the aerodynamic and the inertia components of tail loads decrease with an increase in altitude resulting in lower values of bending moment and torque at all values of displacement gain, K_θ. Figure 5 also illustrates that increasing K_θ has less effect on changing the magnitude of the tail loads at the higher altitude than it does at the lower altitude.

Effect of changing the servo-system characteristic time.- Figures 6 and 7 contain plots of responses against displacement gain for flight conditions I, IV, and V and show the effects of changing servosystem characteristic (or lag) time at one airplane c.g. position and one cruise altitude. Lag times of 0, 0.037, and 0.094 second are examined. In figure 6, $K_{\dot{\theta}} = 0$ and in figure 7, $K_{\dot{\theta}} = 10$. The shapes of the response curves for nonzero lag times (flight conditions IV and V) follow the curves for zero lag time (flight condition I) very closely up to K_θ of approximately 1. At values of K_θ between 1 and 10 (depending on the values of $K_{\dot{\theta}}$ and t_{ch}) the pitch-mode dynamic instability is encountered. The responses then exhibit the characteristic rapid increase with increasing displacement gain and depart from the response curves for zero lag time. The effect of increasing servosystem lag times is to restrict the range of K_θ available before the pitch mode becomes unstable. The restricted range of displacement gains also limits the amount of pitch control available from the autopilot. This limitation is not entirely detrimental since the tail loads are smallest in this K_θ range. The effect of adding rate feedback to the system is beneficial from two standpoints: it increases the K_θ range (delays the onset of instability) and it reduces the magnitudes of all responses.

The selection of the proper combination of displacement and rate gains requires the consideration of numerous criteria such as the effects of structural flexibility and unsteady flow, effects on ride quality, and handling qualities, as well as pitch-attitude disturbance and loads on the wing and the tail. These criteria are all dependent to some extent on the frequencies of the various natural modes of the airplane autopilot system. For the cases of nonzero servosystem lag times, the natural frequencies of the rigid airframe modes and servosystem modes are well separated from the frequencies which excite structural modes and from frequencies in which unsteady-flow effects are significant. These airframe and servosystem frequencies also provide satisfactory ride and handling qualities for passengers and pilots for all combinations of gains within the stability boundary. For the highly idealized cases of zero servosystem lag time, however, the natural frequency of the pitch mode becomes very high with increasing displacement gain. In this higher frequency range, the effects of structural flexibility and unsteady flow must be considered. Flexibility effects may be significant for values of K_θ of 20 and higher. From figure 2, for K_θ equal to 20, the pitch-mode damped natural frequency is approximately 5 hertz, a frequency near the frequencies of the lowest structural modes of a small corporate jet transport. Also, in the higher frequency range there is a phase lag and attenuation of gust forces due to unsteady-flow effects. This phase lag and attenuation would result in turbulence responses lower than those presented for values of K_θ of about 10 and higher.

It is anticipated that ride quality during flight in turbulence would be adversely affected by the use of values of K_θ in the range from 5 to 10 unless large amounts of rate damping, $K_{\dot{\theta}}$, could be applied. For this range of values of K_θ, the pitch-mode frequency falls in the range of about 3 to 5 hertz, which is a frequency range found to be very annoying for human passengers. Handling qualities (how the airplane "feels" to a pilot) are also affected by the choice of gains. Generally, pilots prefer an airplane with a pitching-mode natural frequency that is in the vicinity of 1/2 to 1 hertz, together with a nearly critically damped motion. As indicated in figure 2, the associated value of K_θ may be about 1.0 or less. The corresponding value of damping ratio is only 0.22, however. Adding $K_{\dot{\theta}}$ to the system provides additional damping preferred by pilots and lowers the magnitudes of all responses as well.

Altitude-Control Mode

The purpose of the altitude-control autopilot is to maintain a constant altitude through altitude-perturbation feedback. The effects of varying K_h on airframe and tail-load responses are investigated for various flight conditions. The responses of interest in this autopilot mode are altitude perturbation, c.g. normal acceleration, horizontal-tail bending moment, and horizontal-tail torque.

The characteristic motions for zero servosystem lag time become unstable at a finite value of K_h. For small values of K_h, the phugoid mode is essentially the same as that for the basic airplane but, as K_h increases, the phugoid mode transforms into a slowly decaying long-period oscillatory mode with a strong pitching component and lesser amounts of airspeed and angle-of-attack components. It is this long-period phugoid-type mode which becomes dynamically unstable with increasing altitude-perturbation feedback gain. For all values of K_h corresponding to a stable system, the short-period mode remains essentially unchanged. Also, for nonzero values of K_h, a slowly decaying mode of motion appears that is predominantly a variation in airspeed.

The characteristic motions for nonzero servosystem lag times become dynamically unstable at progressively lower values of K_h as the lag time is increased.

Figures 8 to 11 contain plots of rms values of airframe responses (denoted by subscripts h and θ) and tail-load responses (denoted by subscripts M_b and T) against altitude perturbation feedback gain in the altitude-control mode. The responses are plotted on the ordinate and the altitude-perturbation feedback gain, K_h, on the abscissa.

The effects of K_h on airframe and tail-load responses for one c.g. position, one cruise altitude, and zero-lag time (flight condition I), are shown in figure 8. The value of altitude-perturbation response for $K_h = 0$ ("basic airplane" condition) is theoretically infinitely large in the absence of the consideration of air-density effects on propulsion.

This infinite excursion in altitude is never realized, of course, but it does indicate that without altitude control a small rigid airplane tends to behave like a particle in the very low-frequency samples of atmospheric turbulence. The minimum value of altitude perturbation occurs at $K_h = 5.5 \times 10^{-5}$, and then the response increases rapidly as the critical value for instability is approached. The c.g. normal acceleration and tail-load responses are invariant with K_h up to the onset of instability, at which point they too increase rapidly. The reason for the invariance of the acceleration and tail-load responses with gain at the small values of gain is the following: these responses are produced essentially by the response of the short-period mode which is not changed with changes in altitude-perturbation feedback gain. Thus, there is a range of K_h in which the altitude is controlled effectively, the normal acceleration and tail loads remain unchanged, and an adequate margin from the critical value for instability is maintained.

Effect of changing the airplane center-of-gravity location.- Figure 9 contains responses for flight conditions I and II. The effects of K_h on airframe and tail-load responses for two c.g. locations at constant altitude and zero servosystem lag time are investigated. Since the response of the short-period mode determines the magnitude of the responses (except the altitude perturbation) for the small values of K_h, the effect of a rearward c.g. shift on the short period is of interest. As mentioned in the attitude-hold analysis, moving the c.g. rearward has the net effect of reducing pitch response in the short-period mode which tends to increase the c.g. normal acceleration and tail-load responses. This trend also appears in the altitude-control mode for the entire stable range of K_h. In addition, moving the c.g. rearward decreases, by almost a factor of two, the critical value of K_h for instability. At the rear c.g. position, then, only half the K_h range is available for altitude control. Even with a reduced K_h range, however, the rms value of attitude perturbation reaches a minimum value approximately equal to that attained at the forward c.g. position. The altitude-control autopilot is effective at both c.g. positions without increases in c.g. normal acceleration or tail-load responses.

Effect of changing cruise altitude.- Figure 10 contains responses for flight conditions I and III. The effects of K_h on airframe and tail-load responses for two cruise altitudes at a specific c.g. location are investigated. Again, servosystem lag time is zero. Increasing altitude causes a reduction in air density which significantly reduces c.g. normal acceleration and tail-load responses for all values of K_h. The value of K_h which drives the long-period mode unstable increases by nearly a factor of four with increasing altitude and, as a result, more gain is required to control altitude at the higher altitude.

Unlike the effects of changing the c.g., for which a single gain ($K_h = 3.4 \times 10^{-5}$) provides satisfactory altitude control and an adequate margin from the unstable condition, the effects of changing altitude do not permit the choice of a single gain. A gain which is satisfactory at the lower altitude is not very effective at the higher altitude, and a gain

that is effective at the higher altitude will result in a dynamic instability as altitude is reduced. A need for a K_h that is programed as a function of altitude is indicated.

Effect of changing the servosystem characteristic time.- Figure 11 contains plots of responses against altitude-perturbation feedback gain for flight conditions I, IV, and V and shows the effects of changing servosystem characteristic (or lag) time at one airplane c.g. position and one cruise altitude. Lag times of 0, 0.037, and 0.094 second are examined. The primary effect of increasing the lag time is to reduce the value of K_h which drives the long-period mode unstable. Except near the onset of instability, the shapes of the response curves for nonzero lag times (flight conditions IV and V) are identical to the shapes of the response curves for zero lag time (flight condition I). Even with the reduced K_h range, increasing the lag time does not affect the extent to which altitude is maintained. The minimum values of altitude perturbation response for nonzero lag times are nearly equal to the minimum value of altitude perturbation for zero lag time.

The effects of flexibility and unsteady flow are not significant in the altitude control mode due to the very low natural frequencies associated with the controlled quantity. Ride and handling qualities appear to be adversely affected only when the dynamic instability of the long-period mode is approached too closely.

CONCLUSIONS

A study has been made to assess the loads incurred on the horizontal tail of an autopilot-controlled rigid airplane flying in one-dimensional atmospheric turbulence. The root-mean-square values of rigid-airframe responses and tail-load responses were calculated for three servosystem representations, two airplane center-of-gravity positions, and two cruise altitudes in both pitch-attitude-hold and altitude-control modes. The behavior of the responses was observed for variations in the three autopilot gains.

Attitude-Hold Mode

The following conclusions can be drawn from the results of the attitude-hold analysis:

1. Increasing pitch-displacement feedback gain, K_θ, reduced the rms pitch response but increased c.g. normal-acceleration and tail-load responses.

2. In general, the addition of pitch-rate feedback gain, $K_{\dot{\theta}}$, added damping to the system and reduced the rigid-airframe responses and tail-load responses over the range of K_θ.

3. The shapes of the response curves and their relative magnitudes do not change with changes in c.g. position or changes in cruise altitude.

4. First-order time-lag representation of servosystem dynamics resulted in an unstable pitch mode with increasing K_θ. The instability limited the amount of K_θ useful for control.

5. A combination of K_θ and $K_{\dot{\theta}}$ is available for all servosystem characteristic times which reduces pitch response with very little degradation in c.g. normal acceleration and tail-load responses relative to those of the "basic airplane" condition.

Altitude-Control Mode

The following conclusions can be drawn from the results of the altitude-control analysis:

1. For all low-altitude conditions investigated, with zero servosystem lag time, a value of altitude-perturbation feedback gain, K_h, exists which reduces altitude-perturbation response to a minimum without increasing c.g. normal acceleration or tail-load responses. For the high-altitude condition, with zero lag time, the tail-torque response increases about 25 percent at the gain corresponding to minimum altitude perturbation response.

2. Increasing K_h eventually results in the long-period mode becoming unstable. Decreasing altitude, moving the c.g. rearward, and increasing servosystem characteristic time all result in reduced K_h range because of the long-period mode instability.

3. Gain K_h must be changed with altitude to avoid the long-period mode instability and to maintain effectiveness.

4. Changes in c.g. position and cruise altitude have greater effects on the shapes of the response curves than changes in servosystem dynamics.

Langley Research Center,
National Aeronautics and Space Administration,
Hampton, Va., July 24, 1973.

APPENDIX A

EQUATIONS OF MOTION

The equations used in the present analysis are essentially the classical equations of dynamic stability available from the literature (refs. 6 and 7) with certain refinements made to describe the specific system under consideration. The refinements to the classical equations are: gust forces are added, aerodynamic forces are applied in a manner to account more accurately for the lag in wing downwash and vertical turbulence component acting at the tail, and effects of the autopilot are included. The axes system in which the equations of motion are written is the stability axes system with origin at the airplane mass center.

Expressed in matrix form, the equations of motion are:

$$[M] \{q\} = \phi \left\{ f_{w_g} \right\} \tag{A1}$$

where M is the coefficient matrix of q, the matrix of generalized coordinates, ϕ is the unsteady lift function, and f_{w_g} is the matrix of vertical-gust forces. The elements of equation (A1) are as follows:

$$M = \begin{bmatrix} 2\mu \frac{\bar{c}}{2u_o} s - C_{x_u} & -C_{x_\alpha} & C_{L,o} & 0 \\ 2C_{L,o} - C_{z_u} & 2\mu \frac{\bar{c}}{2u_o} s - C_{z_\alpha} - C_{z_{\dot{\alpha}}} \frac{\bar{c}}{2u_o} s \boxed{\frac{1 - e^{-\tau s}}{\tau s}} & -2\mu \frac{\bar{c}}{2u_o} s - C_{z_q} \frac{\bar{c}}{2u_o} s & -C_{z_\delta} \\ -C_{m_u} & -C_{m_\alpha} - C_{m_{\dot{\alpha}}} \frac{\bar{c}}{2u_o} s \boxed{\frac{1 - e^{-\tau s}}{\tau s}} & i_B \frac{\bar{c}^2}{4u_o^2} s^2 - C_{m_q} \frac{\bar{c}}{2u_o} s & -C_{m_\delta} \\ 0 & \frac{1}{st_{ch} + 1} K_h u_o \frac{1}{s} & \frac{1}{st_{ch} + 1} \left(K_\theta + K_{\dot{\theta}} s - K_h u_o \frac{1}{s} \right) & -1 \end{bmatrix} \tag{A2}$$

The generalized coordinates are

$$q = \begin{Bmatrix} \hat{u} \\ \alpha \\ \theta \\ \delta \end{Bmatrix} \tag{A3}$$

The unsteady-lift function is assumed equal to unity over the entire frequency range. The matrix of vertical-gust forces is given by

$$f_{w_g} = -\frac{w_g}{u_o} \begin{Bmatrix} C_{x_\alpha} \\ C_{z_\alpha} + \left(C_{z_{\dot{\alpha}}} - C_{z_q}\right)\frac{\bar{c}}{2u_o} s \boxed{\frac{1 - e^{-\tau s}}{\tau s}} \\ C_{m_\alpha} + \left(C_{m_{\dot{\alpha}}} - C_{m_q}\right)\frac{\bar{c}}{2u_o} s \boxed{\frac{1 - e^{-\tau s}}{\tau s}} \\ 0 \end{Bmatrix} \tag{A4}$$

Except for the quantity in boxes in equation (A2), the terms in the first three rows and columns are the classical terms found in the literature. The fourth row and column of equation (A2) contains the autopilot terms and will be discussed subsequently. The terms in equation (A4) are the gust forces written in terms of conventional stability derivatives, and it is assumed that the derivatives C_{z_q}, C_{m_q}, $C_{z_{\dot{\alpha}}}$, and $C_{m_{\dot{\alpha}}}$ represent effects of the tail only. The quantity in boxes in equations (A2) and (A4) introduces the transport time lags of wing downwash and turbulence velocity at the tail.

Aerodynamics

In the classical form of the equations of motion, the transport time lags of vertical gust velocity at the tail and downwash at the tail are approximated by retaining only the first two terms of the series expansions of the time-lag exponentials. In the present analysis the exponentials are retained, and equations (A2) and (A4) will reduce to the classical form if the exponential, $e^{-\tau s}$, is approximated by $1 - \tau s$. No other unsteady-flow effects are employed in the present analysis. The unsteady lift function, φ, is set equal to one over the entire frequency range.

Autopilot

The autopilot consists of motion sensors and hardware to drive the elevator. The elevator is constrained to deflect in response to pitch angle and pitch rate in the attitude-hold mode and in response to perturbations in altitude in the altitude-control mode. Only

one autopilot mode is operated at a time and no automatic trim device is considered. The elevator deflection is defined as follows:

Attitude-hold mode

$$\delta = \frac{1}{st_{ch} + 1} (K_\theta + K_{\dot{\theta}} s)\, \theta \tag{A5}$$

Altitude-control mode

$$\delta = \frac{1}{st_{ch} + 1} K_h \cdot h \tag{A6}$$

where

$$h = \frac{u_o}{s} (\alpha - \theta) \tag{A7}$$

and where $\frac{1}{st_{ch} + 1}$ represents the first-order servosystem dynamics, and t_{ch} is the servosystem characteristic (or lag) time. Physically t_{ch} represents the time required for the servosystem transient response to reach a value equal to $\left(1 - \frac{1}{e}\right)$ of its steady-state value and is typically well below the period of the short-period mode. As the expression for δ appears in the equations of motion (both modes contributing), K_h would equal zero in the attitude-hold mode and K_θ and $K_{\dot{\theta}}$ would equal zero in the altitude-control mode. It is assumed that the hinge moment due to gusts is negligible compared to the other terms in the elevator equation. The last element in equation (A4) is, therefore, equal to zero.

Frequency-response functions describe the responses of the airplane to a unit sinusoidal gust of varying frequencies. Rigid-airframe frequency-response functions are obtained by solving the equations of motion for the generalized coordinates, q, and then substituting $i\omega$ for s. From equation (A1)

$$[M]\ \{q\} = \phi \left\{ f_{w_g} \right\}$$

Solving for the generalized coordinates

$$\{q\} = [M]^{-1}\, \phi \left\{ f_{w_g} \right\}$$

and since $\phi = 1$ for this analysis

$$\{q\} = \begin{Bmatrix} \hat{u}(s) \\ \alpha(s) \\ \theta(s) \\ \delta(s) \end{Bmatrix} = [M]^{-1} \left\{ f_{w_g} \right\} \tag{A8}$$

Substituting $i\omega$ for s in equation (A8) yields the frequency-response functions, and dividing equation (A8) by w_g gives the frequency responses in per unit gust-velocity form, H_{R/w_g}, where R denotes airframe responses $\hat{u}$, α, etc., and tail-load responses V, M_b, and T

$$\begin{Bmatrix} H_{\hat{u}/w_g}(i\omega) \\ H_{\alpha/w_g}(i\omega) \\ H_{\theta/w_g}(i\omega) \\ H_{\delta/w_g}(i\omega) \end{Bmatrix} = [M(i\omega)]^{-1} \frac{1}{w_g} \left[f_{w_g}(i\omega) \right] \tag{A9}$$

The frequency-response functions of c.g. normal acceleration and altitude perturbation per unit gust velocity are

$$H_{a_{c.g.}/g/w_g}(i\omega) = i\omega \frac{u_o}{g} \left[H_{\theta/w_g}(i\omega) - H_{\alpha/w_g}(i\omega) \right] \tag{A10}$$

$$H_{h/w_g}(i\omega) = -\frac{i}{\omega} u_o \left[H_{\alpha/w_g}(i\omega) - H_{\theta/\omega_g}(i\omega) \right] \tag{A11}$$

The frequency responses of $a_{c.g.}$ and h are linear combinations of the frequency responses of α and θ.

Equations (A9) to (A11), in conjunction with equations (1) to (3) in the main body of the paper, provide the rms values of the rigid-airframe responses.

APPENDIX B

TAIL LOADS

The tail loads under consideration in the present analysis are the shear and bending moment at the root of the horizontal tail and the torque about the horizontal-tail elastic axis. All tail loads are comprised of an aerodynamic component and an inertial component, and the tail loads are calculated using simple cantilever-beam theory. The equations presented allow for tail-loads calculations at any spanwise location $y = \bar{y}$. The tail loads at the horizontal-tail root are obtained by letting $\bar{y} = 0$.

The lift on the tail consists of contributions from angle of attack and elevator-deflection angle and provides the aerodynamic component of tail loads. The tail angle of attack

$$\alpha_t = \alpha_w \left(1 - e^{-\tau s} \frac{d\epsilon}{d\alpha}\right) + \frac{\ell_h}{u_o} s\theta + \alpha_g \left(1 - \frac{d\epsilon}{d\alpha}\right) e^{-\tau s} \tag{B1}$$

contains motion terms and gust terms, both with appropriate transport time lags. The expression for elevator deflection angle has already been given in equations (A5) and (A6). The expression for total lift on the horizontal tail is

$$L_t = \frac{1}{2} \rho u_o^2 S_t \left(C_{L_{\alpha_t}} \alpha_t + C_{L_{t_\delta}} \delta\right) \tag{B2}$$

which reduces to $\frac{1}{2} \rho u_o^2 S_t C_{L_{\alpha_t}} \alpha_t$ for the autopilot-off condition. The lift distribution is assumed semielliptical across the span, and the chordwise distributions will be described subsequently.

The mass of the horizontal tail times the acceleration of the horizontal tail provides the inertial component of tail loads. The normal acceleration at the horizontal tail is

$$a_t = a_{c.g.} - \ell_h s^2 \theta \tag{B3}$$

which contains contributions from c.g. normal acceleration and pitching normal acceleration. The mass distribution is assumed trapezoidal along the span and is assumed to be concentrated at the 55-percent-chord position.

Shear

The shear on the horizontal tail is obtained by integrating the spanwise aerodynamic force distribution and the spanwise inertia force distribution over the span of the horizontal tail. Positive shear is defined to be in the positive z-direction. The shear at any spanwise location, $\bar{y}$, is given by

$$V(\bar{y}) = \frac{\int_{y=\bar{y}}^{b_t/2} \ell_t(y)\,dy}{\int_{y=0}^{b_t/2} \ell_t(y)\,dy} \frac{L_t}{2} - \int_{y=\bar{y}}^{b_t/2} m_t(y)\,dy \cdot a_t \qquad \text{(B4)}$$

where $\ell_t(y)$ is the spanwise lift distribution and $m_t(y)$ is the spanwise mass distribution, and L_t is the total lift on the tail and a_t is the normal acceleration at the tail. The quotient of integrals in equation (B4) represents the fraction of the tail lift outboard of spanwise station $\bar{y}$. When $\bar{y} = 0$ the value of the fraction is 1 and the aerodynamic component of shear is then simply half the lift on the tail. The inertial component of shear, when $\bar{y} = 0$, is the product of half the mass of the tail and the acceleration of the tail.

Bending Moment

The bending moment on the horizontal tail is obtained by integrating the spanwise shear distribution over the span, or equivalently, by integrating the products of the aerodynamic and inertial force distributions and their respective moment arms over the span. Bending moment is defined to be positive for a positive shear acting at a positive y arm. The expression for tail bending moment at any spanwise location, $\bar{y}$, is

$$M_b(\bar{y}) = \frac{\int_{y=\bar{y}}^{b_t/2} \ell_t(y)(y-\bar{y})\,dy}{\int_{y=0}^{b_t/2} \ell_t(y)\,dy} \frac{L_t}{2} - \int_{y=\bar{y}}^{b_t/2} m_t(y)(y-\bar{y})\,dy \cdot a_t \qquad \text{(B5)}$$

The quotient of integrals in equation (B5) represents the distance from spanwise station $\bar{y}$ to the centroid of that portion of the spanwise lift distribution outboard of station $\bar{y}$. This distance is the moment arm of the aerodynamic component of bending moment.

Torque

The calculation of torque about the horizontal-tail elastic axis requires two sets of integrations: integrations across the chord and then integration across the span.

The chordwise integrations serve to establish the effective "moment arms" of the various chordwise force distributions from their "centroids" to the horizontal-tail elastic axis. The "moment arms" are expressed as a percentage of the horizontal-tail chord, and this percentage of chord is assumed to be constant along the span. The spanwise integration of the spanwise force distributions times their respective "moment arms" then provides the torque about the elastic axis at any spanwise location $\bar{y}$.

In performing the chordwise integrations, it is necessary to know how the presence of the elevator hinge affects the calculations. It is assumed that the elevator hinge is full-span, nonswept, continuous, and frictionless and can therefore transmit no moments or torques. The following sketches will serve to illustrate how the "moment arms," which result from the chordwise integrations, are obtained:

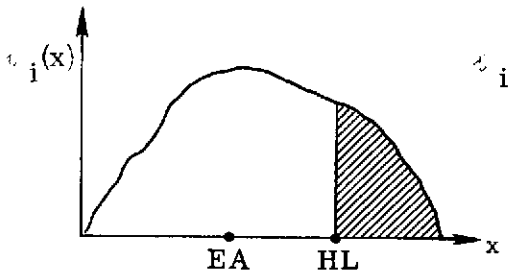

Sketch 1

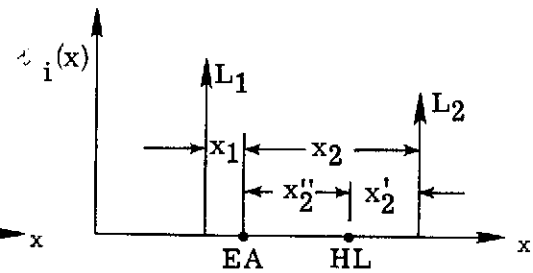

Sketch 2

In sketch 1, $\ell_i(x)$ is a general chordwise force distribution over the horizontal tail which produces a torque, T, about the elastic axis (labeled EA). In sketch 2 the force distribution has been integrated and replaced by two concentrated forces L_1 and L_2 at distances x_1 and x_2 from the elastic axis. These forces, L_1 and L_2, are equal to the forces forward and aft of the hinge line (labeled HL), respectively, and produce the same torque about the elastic axis as the original force distribution produced (assuming a fixed hinge in both instances). The torque about the elastic axis due to L_1 is simply x_1L_1. The torque about the elastic axis due to L_2 (with fixed hinge) is x_2L_2 which is equivalent to $(x_2' + x_2'')L_2$. When the hinge is assumed frictionless (no longer fixed), the torque $x_2' L_2$ cannot be transmitted across the hinge line; therefore, the only contribution to torque about the elastic axis due to L_2 is $x_2''L_2$. The torque about the elastic axis due to both L_1 and L_2 is

$$T = x_1L_1 + x_2'' L_2$$

$$= \left(\frac{x_1L_1 + x_2'' L_2}{\bar{c}_t L} \right) \bar{c}_t L$$

$$= c_i \, \bar{c}_t \, L$$

where L is the sum of L_1 and L_2 and equals the chordwise integral of $\ell_i(x)$, c_i is the effective moment-arm coefficient such that when multiplied by $\bar{c}_t$, the mean aerodynamic chord of the horizontal tail, the product is the effective "moment arm" of distribution $\ell_i(x)$.

For purposes of calculating the torque about the horizontal-tail elastic axis, the chordwise lift distributions (due to α_t and δ) are further broken down by using the notation and method described in the appendix of reference 8. The chordwise lift distribution due to angle of attack is described by $\ell_{a_\alpha}(x)$, the "additional" lift distribution due to α_t. This distribution is equal to the distribution over the horizontal tail when the elevator is not deflected. The chordwise lift distribution due to elevator deflection angle is described by $\ell_{a_\delta}(x)$ and $\ell_{b_\delta}(x)$, the "additional" and "basic" incremental lift distributions due to δ. The sum of $\ell_{a_\delta}(x)$ and $\ell_{b_\delta}(x)$ represents the increase in tail-lift distribution when the elevator is deflected. These chordwise lift distributions are illustrated in figure 12, where ℓ_a represents ℓ_{a_α} or ℓ_{a_δ} and ℓ_b represents ℓ_{b_δ}. The quantities $L_{a_\alpha}(x)$, $L_{a_\delta}(x)$, and $L_{b_\delta}(x)$ represent the chordwise integrations of ℓ_{a_α}, ℓ_{a_δ}, and ℓ_{b_δ}, respectively, and the sum of L_{a_α}, L_{a_δ}, and L_{b_δ} is the total lift on the horizontal tail, L_t. References 8, 9, and 10 provide the method for obtaining L_{a_α}, L_{a_δ}, and L_{b_δ} as fractions of L_t for the particular elevator-chord ratio used in this analysis.

It is now possible to write the torque equation. Torque about the horizontal-tail elastic axis is defined to be positive counterclockwise when viewed from the left side of the airplane. The torque at any spanwise location, $\bar{y}$, is given by

$$T(\bar{y}) = \frac{\int_{y=\bar{y}}^{b_t/2} c_1 c_t(y)\, \ell_{a_\alpha}(y)\, dy}{\int_{y=0}^{b_t/2} \ell_{a_\alpha}(y)\, dy} \frac{L_{a_\alpha}}{2} + \frac{\int_{y=\bar{y}}^{b_t/2} c_2 c_t(y)\, \ell_{a_\delta}(y)\, dy}{\int_{y=0}^{b_t/2} \ell_{a_\delta}(y)\, dy} \frac{L_{a_\delta}}{2}$$

$$+ \frac{\int_{y=\bar{y}}^{b_t/2} c_3 c_t(y)\, \ell_{b_\delta}(y)\, dy}{\int_{y=0}^{b_t/2} \ell_{b_\delta}(y)\, dy} \frac{L_{b_\delta}}{2} + \int_{y=\bar{y}}^{b_t/2} c_4 c_t(y) m_t(y)\, dy \cdot a_t \qquad \text{(B6)}$$

The products $c_i \cdot c_t(y)$, where $i = 1 \ldots 4$, are the effective "moment arms" of the chordwise distributions, and they are expressed as fractions of the local horizontal-tail chord. The terms $\ell_{a_\alpha}(y)$, $\ell_{a_\delta}(y)$, and $\ell_{b_\delta}(y)$ are assumed to be semielliptical across the span.

Frequency-response functions of the tail loads and associated responses are obtained in the same manner as the frequency-response functions in appendix A. Frequency responses for tail angle of attack, tail lift, and tail normal acceleration are expressed as linear combinations of the rigid-airframe frequency responses. The tail-load frequency responses are then expressed as linear combinations of tail lift and tail normal acceleration.

From equations (B1) to (B3)

$$H_{\alpha_t/w_g}(i\omega) = \left(1 - e^{-i\omega\tau}\frac{d\epsilon}{d\alpha}\right)H_{\alpha/w_g}(i\omega) + i\omega\frac{\ell_h}{u_o}H_{\theta/w_g}(i\omega) - \frac{1}{u_o}\left(1 - \frac{d\epsilon}{d\alpha}\right)e^{-i\omega\tau} \quad \text{(B7)}$$

$$H_{L_t/w_g}(i\omega) = \frac{1}{2}\rho u_o^2 S_t\left(C_{L_{\alpha_t}}H_{\alpha_t/w_g}(i\omega) + C_{L_{t_\delta}}H_{\delta/w_g}(i\omega)\right) \quad \text{(B8)}$$

$$H_{a_t/w_g}(i\omega) = gH_{a_{c.g./g}/w_g}(i\omega) + \ell_h\omega^2 H_{\theta/w_g}(i\omega) \quad \text{(B9)}$$

The frequency-response functions for the tail loads become

$$H_{V/w_g}(i\omega) = \frac{\int_{y=\bar{y}}^{b_t/2}\ell_t(y)\,dy}{\int_{y=0}^{b_t/2}\ell_t(y)\,dy}\frac{1}{2}H_{L_t/w_g}(i\omega) - \int_{y=\bar{y}}^{b_t/2}m_t(y)\,dy\,H_{a_t/w_g}(i\omega) \quad \text{(B10)}$$

$$H_{M_b/w_g}(i\omega) = \frac{\int_{y=\bar{y}}^{b_t/2} \ell_t(y)(y-\bar{y})\,dy}{\int_{y=0}^{b_t/2} \ell_t(y)\,dy} \frac{1}{2} H_{L_t/w_g}(i\omega) - \int_{y=\bar{y}}^{b_t/2} m_t(y)(y-\bar{y})dy\, H_{a_t/w_g}(i\omega) \tag{B11}$$

$$H_{T/w_g}(i\omega) = \frac{\int_{y=\bar{y}}^{b_t/2} c_1 c_t(y) \ell_{a_\alpha}(y)\,dy}{\int_{y=0}^{b_t/2} \ell_{a_\alpha}(y)\,dy} \frac{1}{2} H_{L_{a_\alpha}/w_g}(i\omega)$$

$$+ \frac{\int_{y=\bar{y}}^{b_t/2} c_2 c_t(y)\, \ell_{a_\delta}(y)\,dy}{\int_{y=0}^{b_t/2} \ell_{a_\delta}(y)\,dy} \frac{1}{2} H_{L_{a_\delta}/w_g}(i\omega)$$

$$+ \frac{\int_{y=\bar{y}}^{b_t/2} c_3 c_t(y) \ell_{b_\delta}(y)\,dy}{\int_{y=0}^{b_t/2} \ell_{b_\delta}(y)\,dy} \frac{1}{2} H_{L_{b_\delta}/w_g}(i\omega)$$

$$+ \int_{y=\bar{y}}^{b_t/2} c_4 c_t(y) m_t(y)\,dy\, H_{a_t/w_g}(i\omega) \tag{B12}$$

Equations (B7) to (B12), in conjunction with equations (1) to (3) in the main body of the paper, provide the rms values of the tail loads and associated responses.

REFERENCES

1. Porter, Richard F.; Loomis, James P.; and Robinson, Alfred C.: A Procedure for Assessing Aircraft Turbulence-Penetration Performance. NASA CR-1510, 1970.
2. Oehman, Waldo I.: An Analytical Study of Airplane-Autopilot Response to Atmospheric Turbulence. NASA TN D-6869, 1972.
3. Blakelock, John H.: Automatic Control of Aircraft and Missiles. John Wiley & Sons, Inc., c.1965.
4. Houbolt, John C.; Steiner, Roy; and Pratt, Kermit G.: Dynamic Response of Airplanes to Atmospheric Turbulence Including Flight Data on Input and Response. NASA TR R-199, 1964.
5. Pratt, Kermit G.: Response of Flexible Airplanes to Atmospheric Turbulence. Performance and Dynamics of Aerospace Vehicles, NASA SP-258, 1971, pp. 439-503.
6. Etkin, Bernard: Dynamics of Flight. John Wiley & Sons, Inc., c.1959.
7. Dodd, H. M., Jr.; and Pratt, G.: T-Tail Empennage Loads in Continuous Atmospheric Turbulence. J. Aircraft, vol. 8, no. 8, Aug. 1971, pp. 616-622.
8. Allen, H. Julian: Calculation of the Chordwise Load Distribution Over Airfoil Sections With Plain, Split, or Serially Hinged Trailing-Edge Flaps. NACA Rep. 634, 1938.
9. Jones, Robert T.; and Cohen, Doris: An Analysis of the Stability of an Airplane With Free Controls. NACA Rep. 709, 1941.
10. Wood, Karl D.: Technical Aerodynamics. First ed., McGraw-Hill Book Co., Inc., 1935.

TABLE I.- AIRPLANE CHARACTERISTICS

Mass of airplane, m, kg	7860
Mass moment of inertia about pitch axis, I_{yy}, kg m^2	27 600
Wing area, S, m^2	31.8
Mean aerodynamic chord of wing, $\bar{c}$, m	2.55
Sweep angle of wing quarter-chord, $\Lambda_{.25\bar{c}}$, deg	28.6
Nondimensional tail length, $\ell_h/\bar{c}$	2.6
Horizontal-tail area, S_t, m^2	7.15
Mean aerodynamic chord of horizontal tail, $\bar{c}_t$, m	1.47
Sweep angle of horizontal-tail elastic axis, Λ_{EA}, deg	0
Elevator chord ratio	0.35
$d\epsilon/d\alpha$	0.566

TABLE II.- FLIGHT CONDITIONS

[Mach number was equal to 0.75 for all flight conditions]

Flight condition	Cruise altitude, m	c.g. position, percent $\bar{c}$	Servosystem characteristic time, sec
I	6 100	27	0
II	6 100	31	0
III	12 200	27	0
IV	6 100	27	.037
V	6 100	27	.094

TABLE III.- STABILITY DERIVATIVES

Stability derivatives	Flight conditions		
	I, IV, V	II	III
C_{x_u}	-0.0642	-0.0642	-0.0993
C_{x_α}	.039	.039	.086
$C_{L,o}$	.133	.133	.332
C_{z_u}	-.171	-.171	-.427
$C_{z_{\dot{\alpha}}}$	-2.46	-2.41	-2.46
C_{z_α}	-5.62	-5.62	-5.93
C_{z_q}	-4.35	-4.25	-4.35
C_{z_δ}	-.472	-.472	-.472
C_{m_u}	0	0	0
$C_{m_{\dot{\alpha}}}$	-6.47	-6.18	-6.47
C_{m_α}	-.841	-.616	-.841
C_{m_q}	-11.44	-10.92	-11.44
C_{m_δ}	-1.24	-1.21	-1.24

TABLE IV.- RESULTS OF STABILITY ANALYSIS

Flight condition	Servosystem characteristic time, sec	Attitude-hold mode		Altitude-control mode
		K_θ ($K_{\dot{\theta}} = 0$)	K_θ ($K_{\dot{\theta}} = 10$)	K_h
I	0	∞	∞	7.5×10^{-5}
II	0	∞	∞	4.5×10^{-5}
III	0	∞	∞	3.7×10^{-4}
IV	.037	2.6	4.1	6.4×10^{-5}
V	.094	1.5	2.3	5.4×10^{-5}

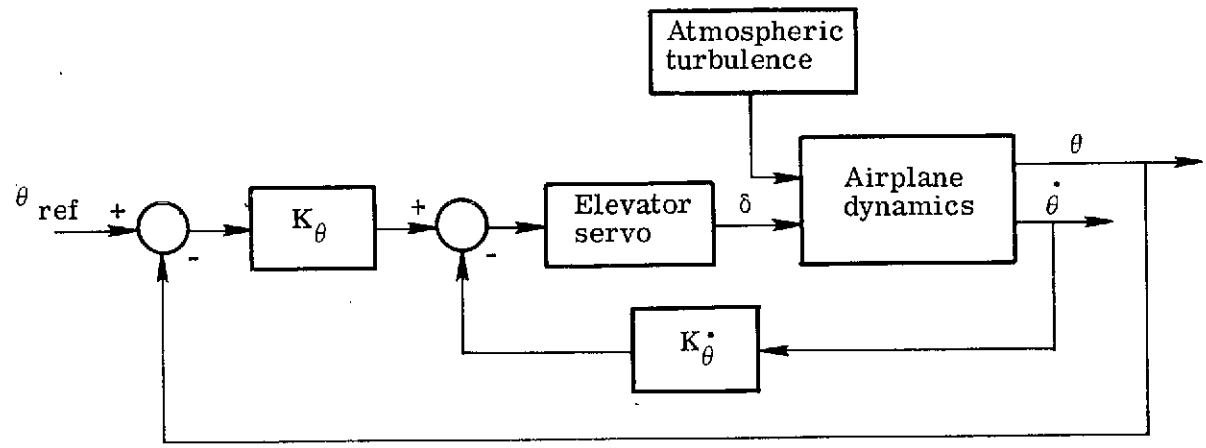

(a) Attitude-hold autopilot.

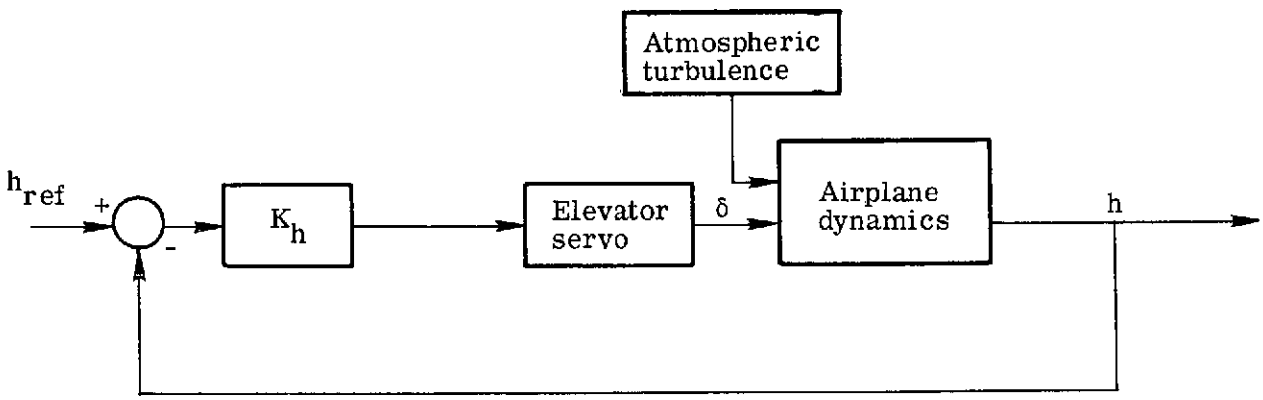

(b) Altitude-control autopilot.

Figure 1.- Block diagrams of airplane autopilot system.

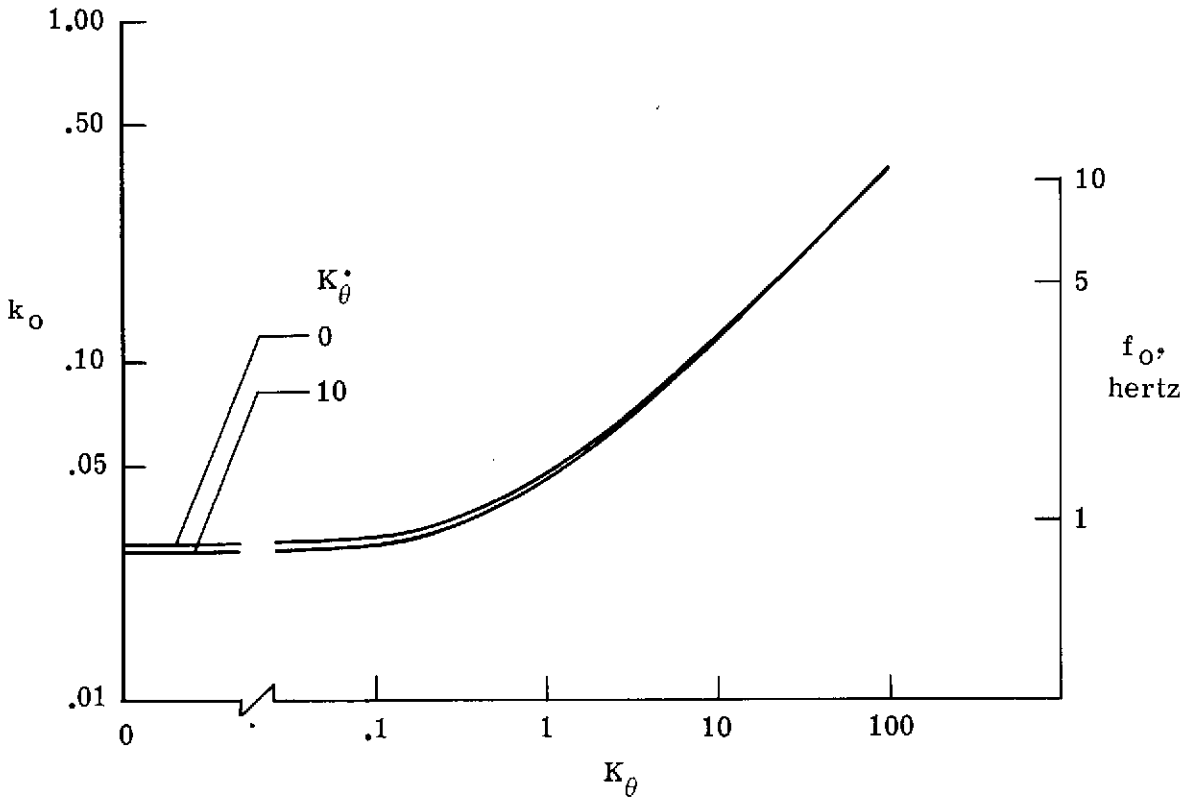

Figure 2.- Variation of pitch-mode natural frequency with pitch-displacement feedback gain, K_θ. $(t_{ch} = 0.)$

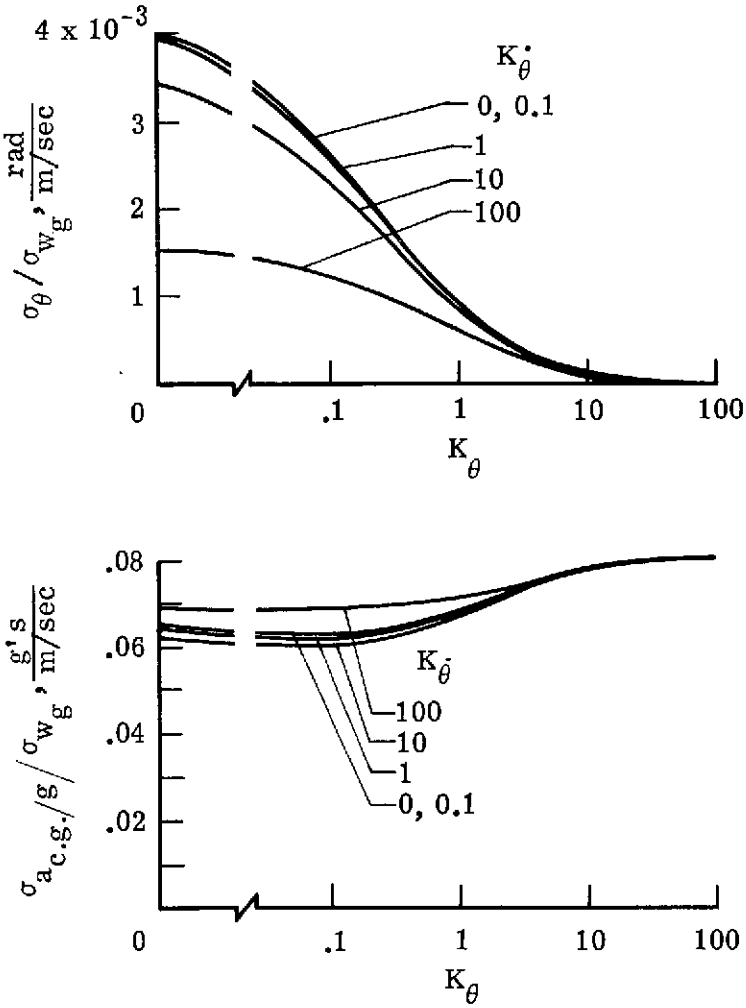

Figure 3.- The effects of pitch-displacement and pitch-rate feedback gains, K_θ and $K_{\dot{\theta}}$, on airframe and tail-load responses. Flight condition I (table II).

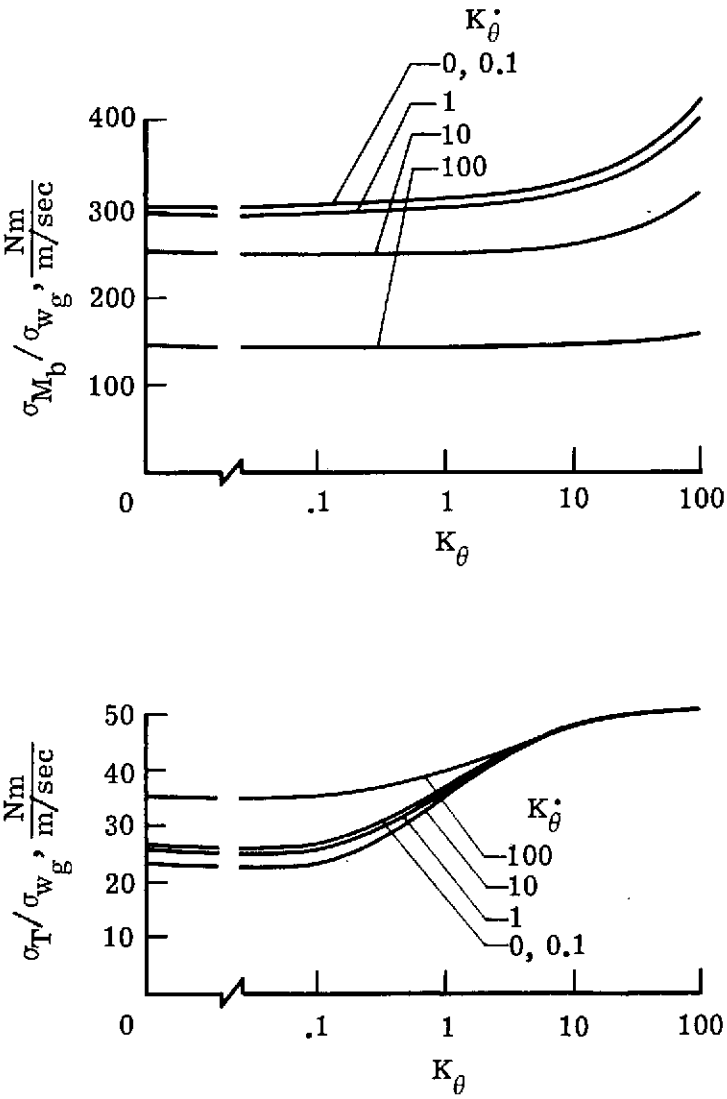

Figure 3.- Concluded.

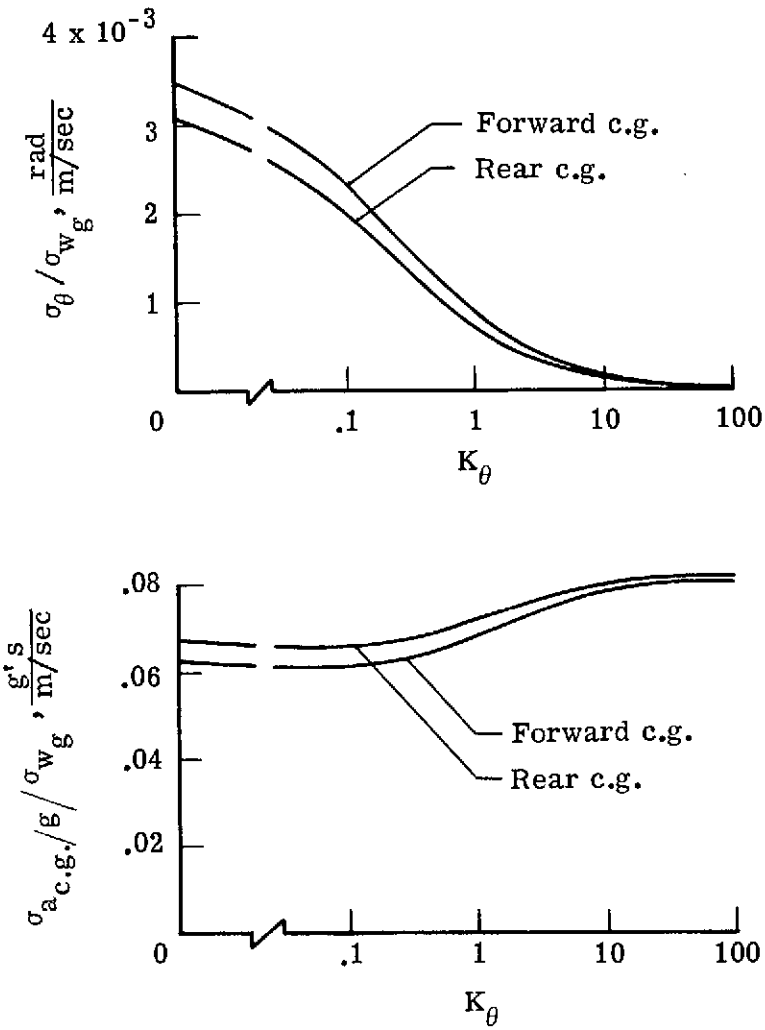

Figure 4.- The effects of pitch-displacement feedback gain, K_θ, on airframe and tail-load responses for two airplane c.g. locations. Flight conditions I and II (table II). ($K_{\dot{\theta}} = 10.$)

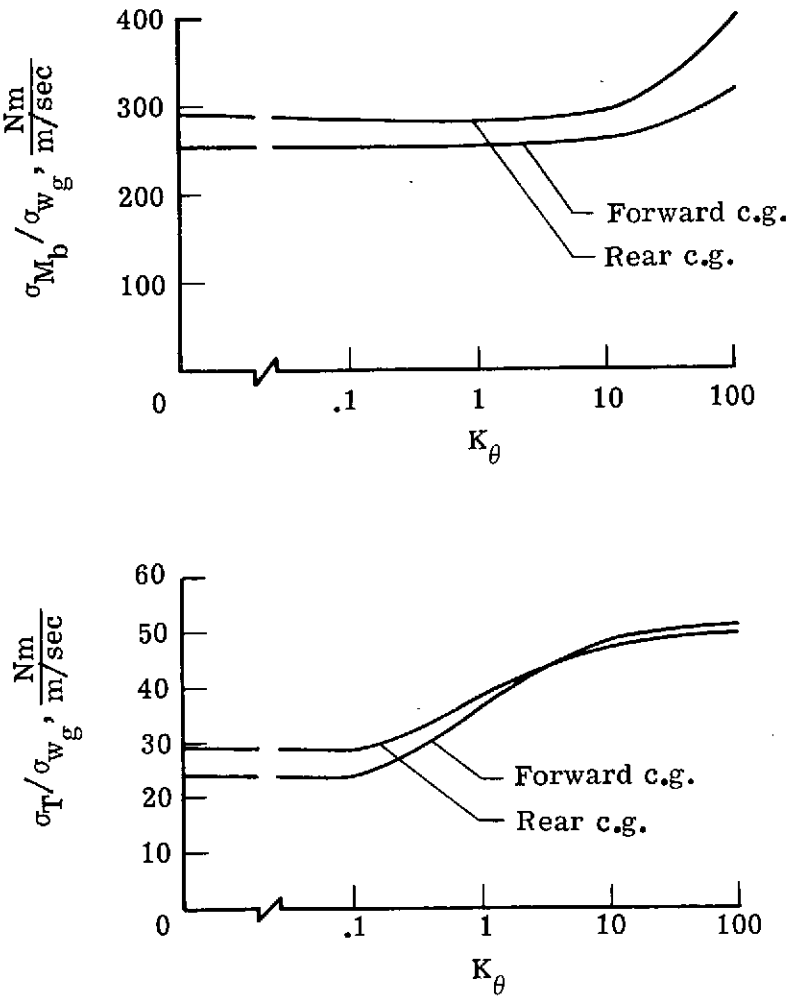

Figure 4.- Concluded.

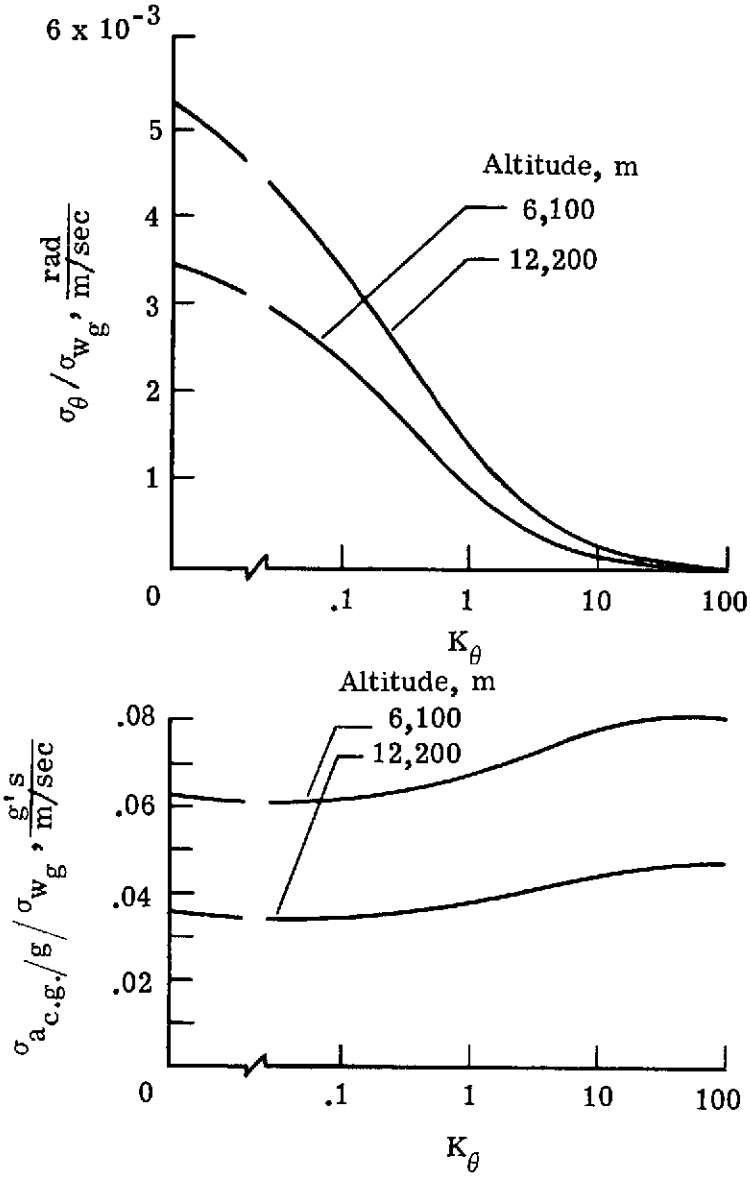

Figure 5.- The effects of pitch-displacement feedback gain, K_θ, on airframe and tail-load responses for two cruise altitudes. Flight conditions I and III (table II). ($K_{\dot{\theta}} = 10.$)

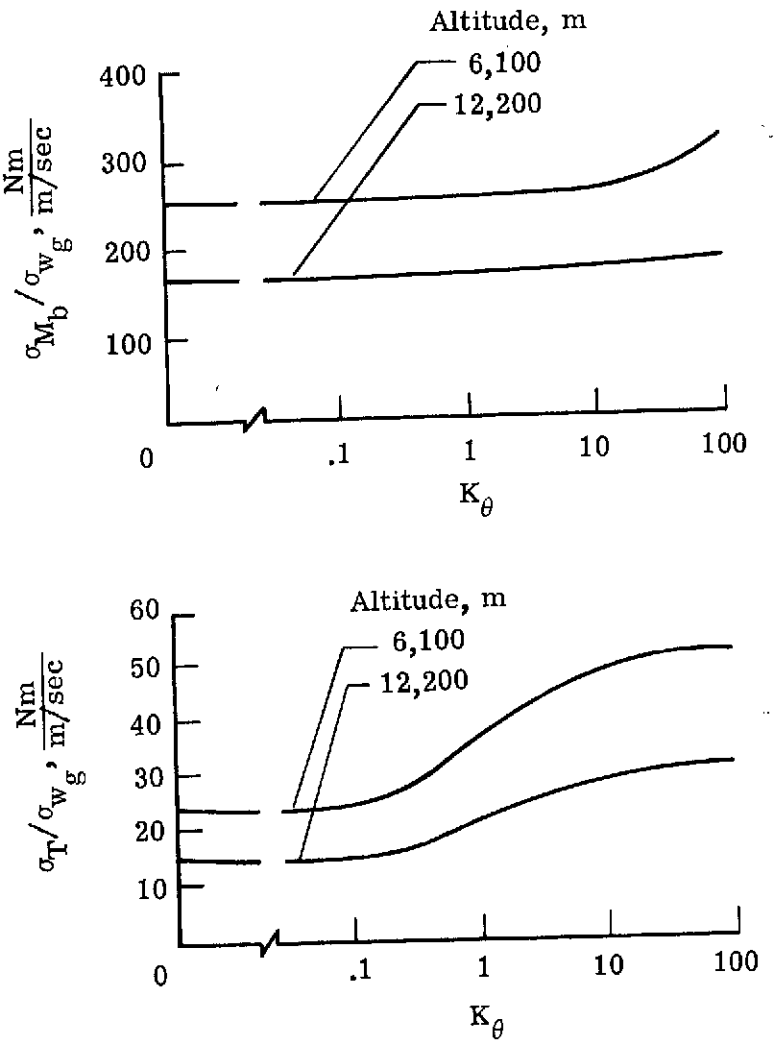

Figure 5.- Concluded.

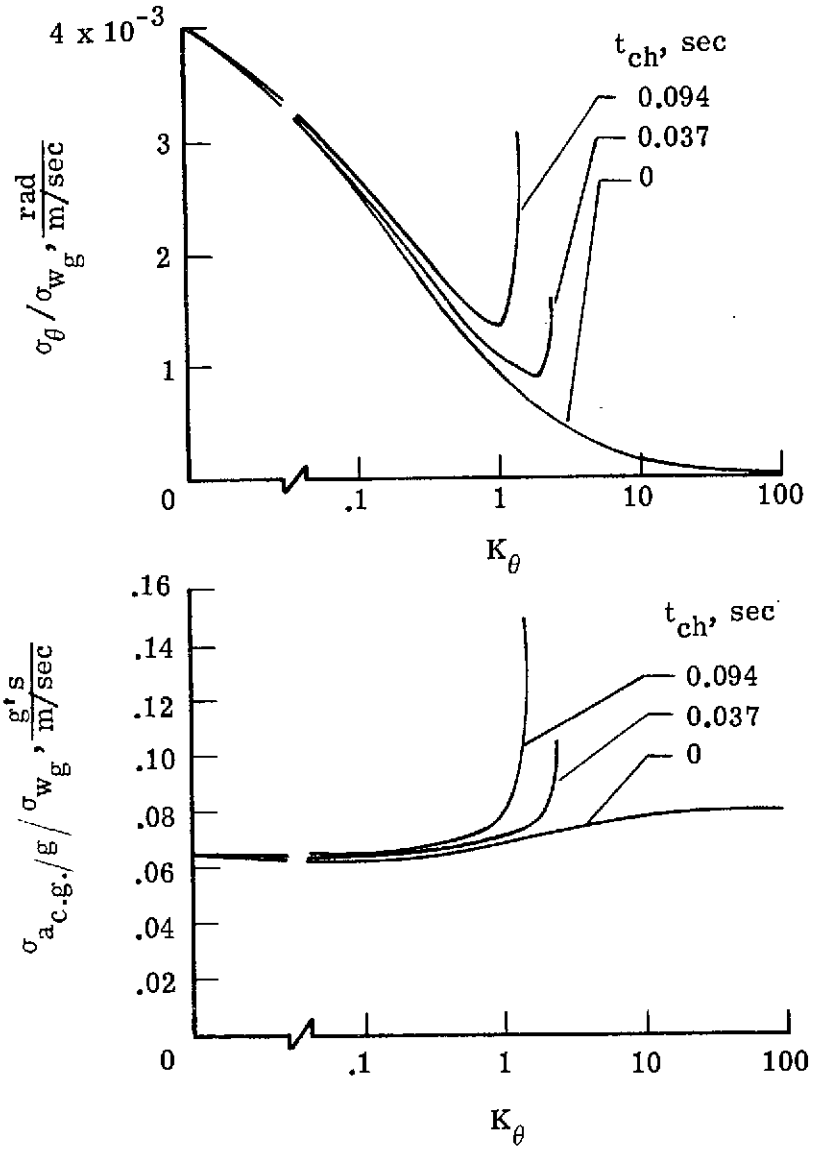

Figure 6.- The effects of pitch-displacement feedback gain, K_θ, on airframe and tail-load responses for three servosystem lag times. Flight conditions I, IV, and V (table II). ($K_{\dot{\theta}} = 0.$)

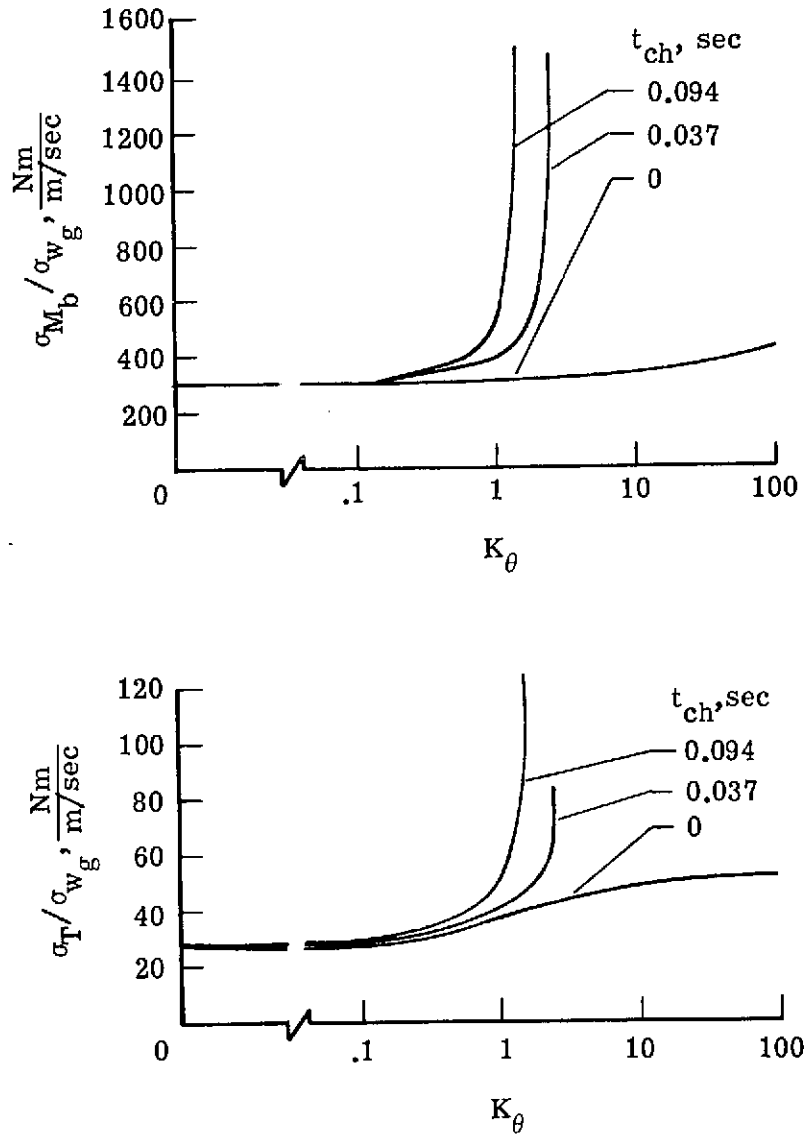

Figure 6.- Concluded.

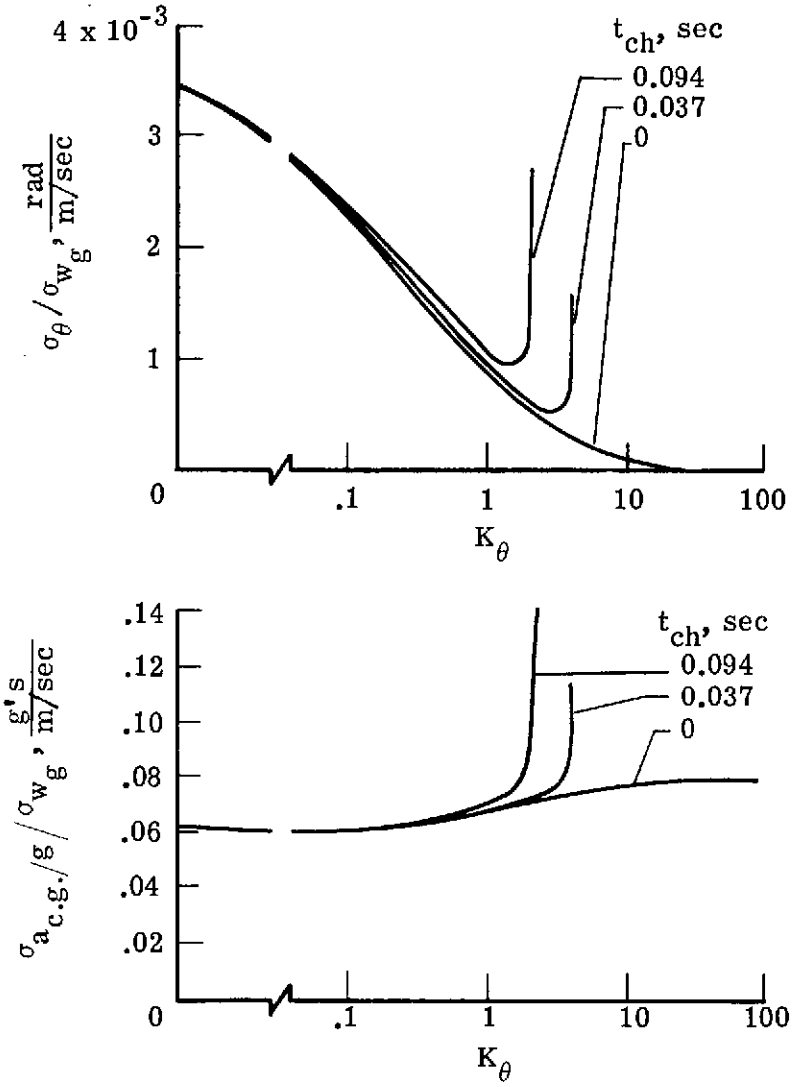

Figure 7.- The effects of pitch-displacement feedback gain, K_θ, on airframe and tail-load responses for three servosystem lag times. Flight conditions I, IV, and V (table II). ($K_{\dot{\theta}} = 10.$)

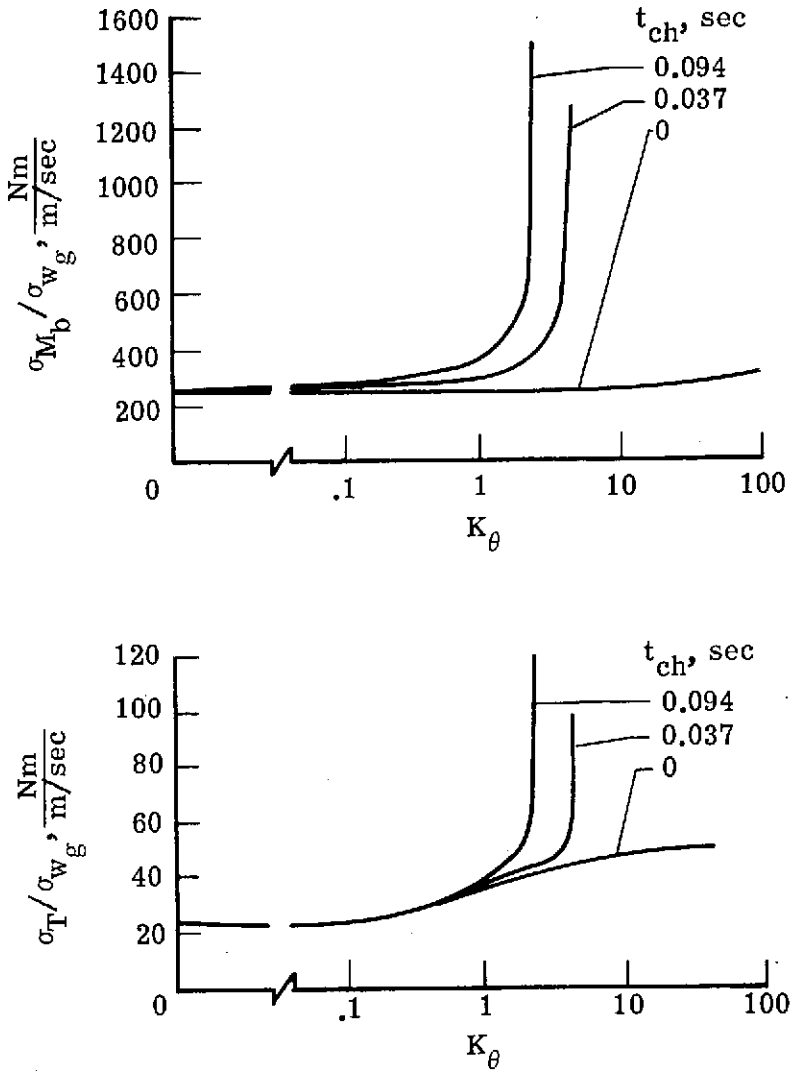

Figure 7.- Concluded.

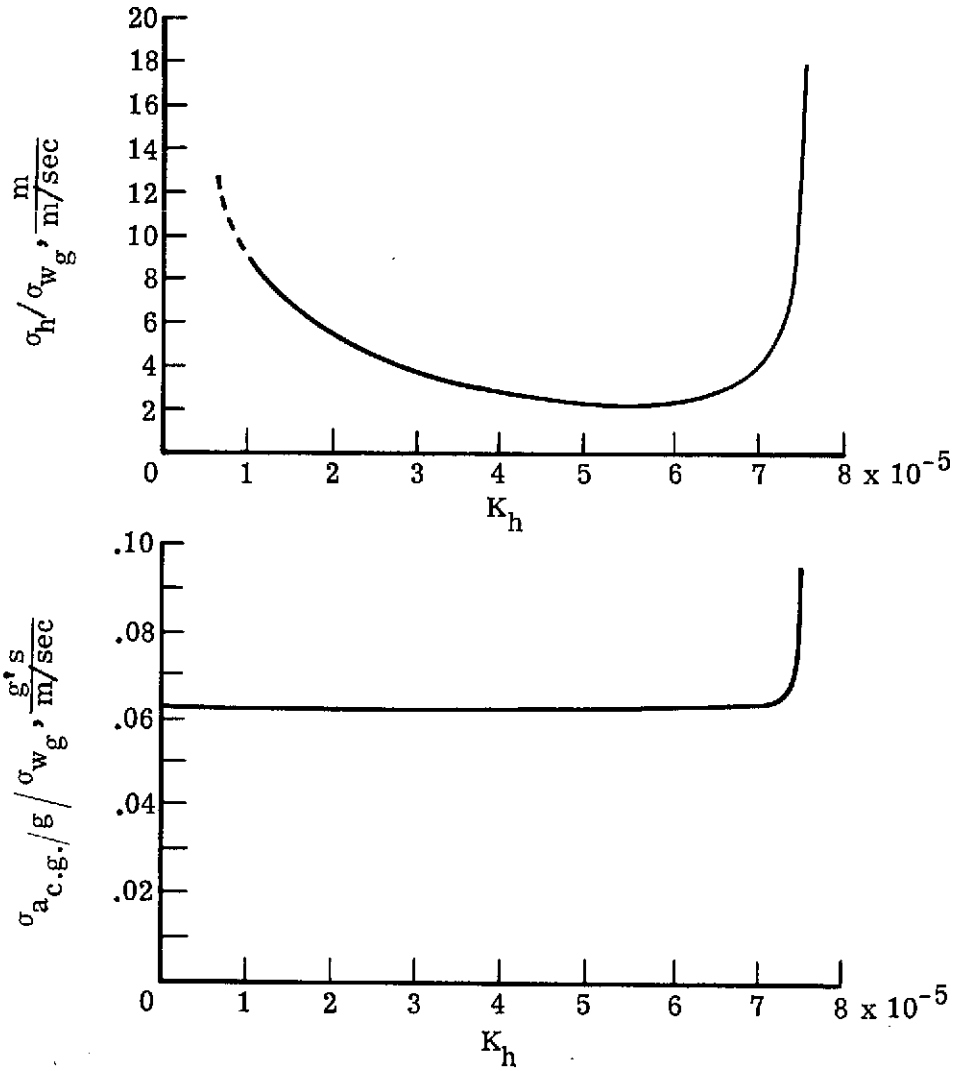

Figure 8.- The effects of altitude-perturbation feedback gain, K_h, on airframe and tail-load responses. Flight condition I (table II).

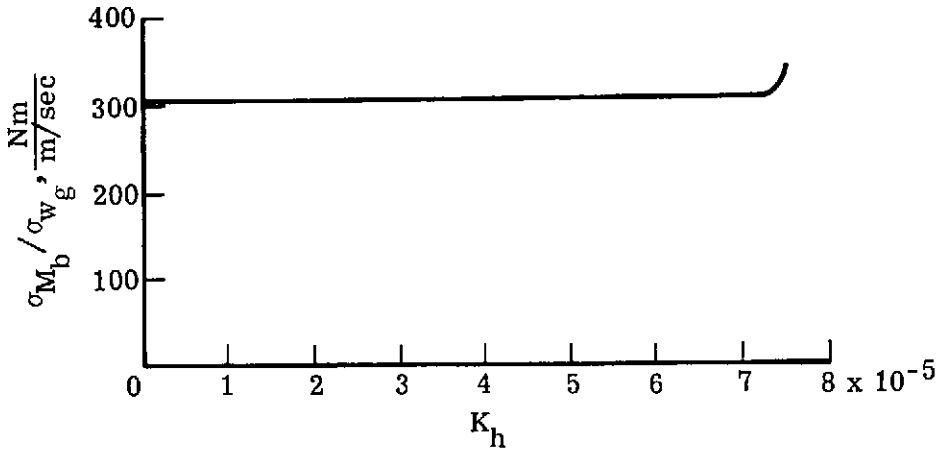

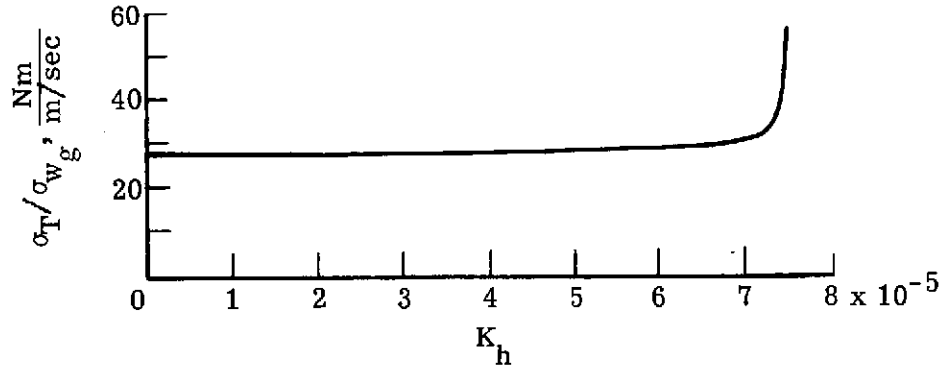

Figure 8.- Concluded.

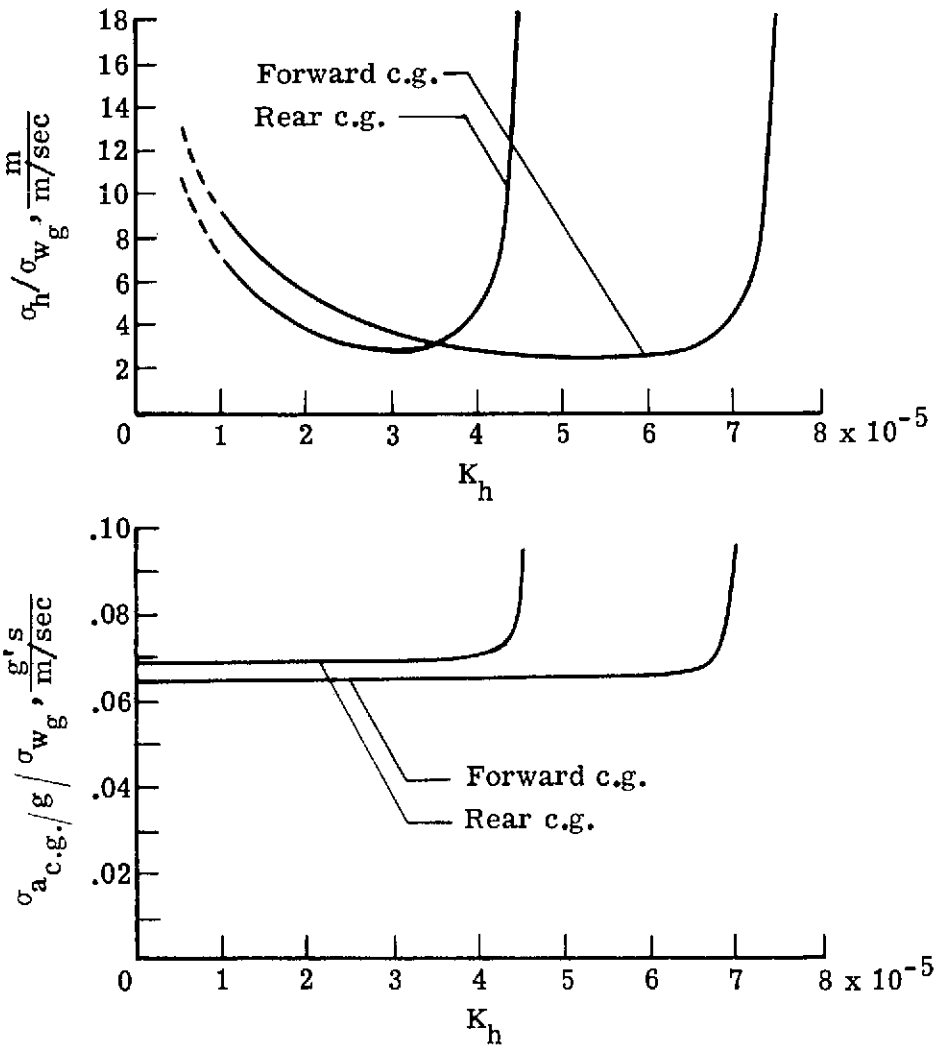

Figure 9.- The effects of altitude-perturbation feedback gain, K_h, on airframe and tail-load responses for two airplane c.g. locations. Flight conditions I and II (table II).

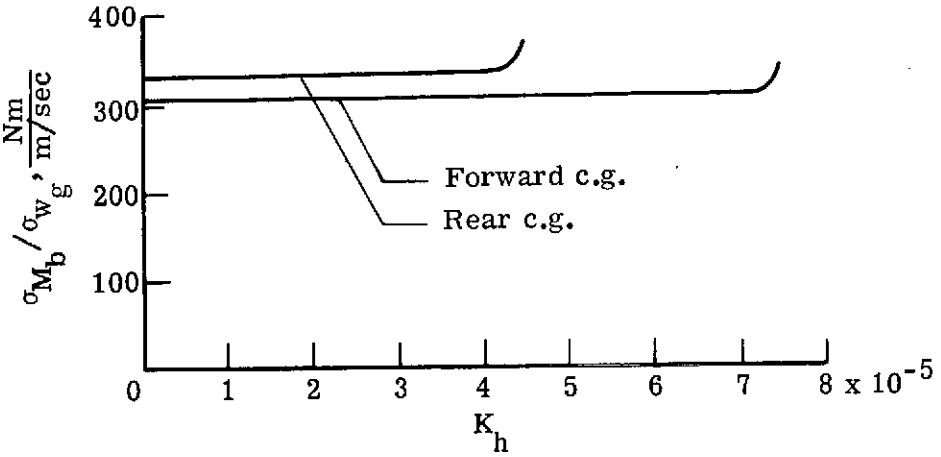

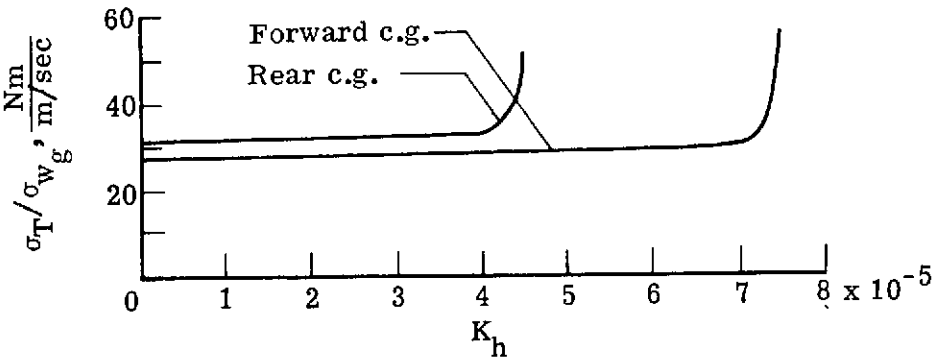

Figure 9.- Concluded.

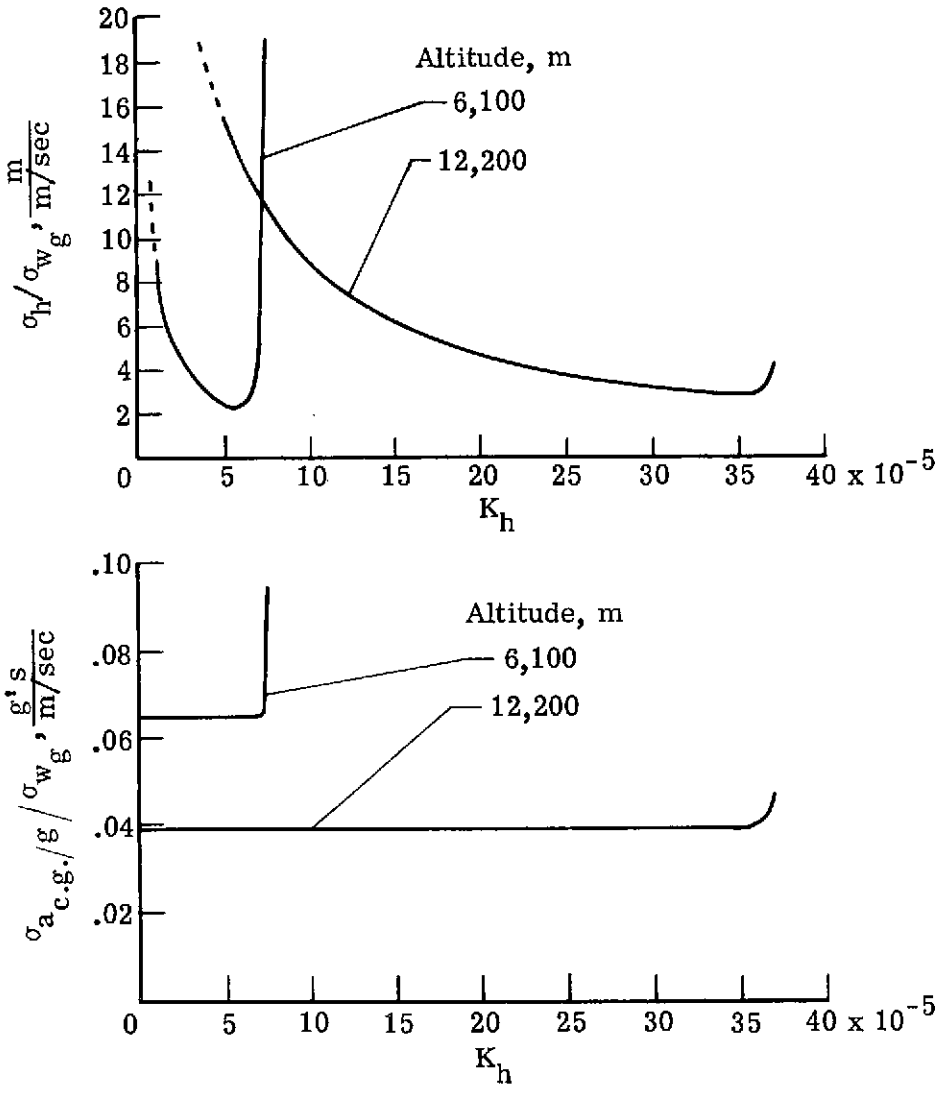

Figure 10.- The effects of altitude-perturbation feedback gain, K_h, on airframe and tail-load responses for two cruise altitudes. Flight conditions I and III (table II).

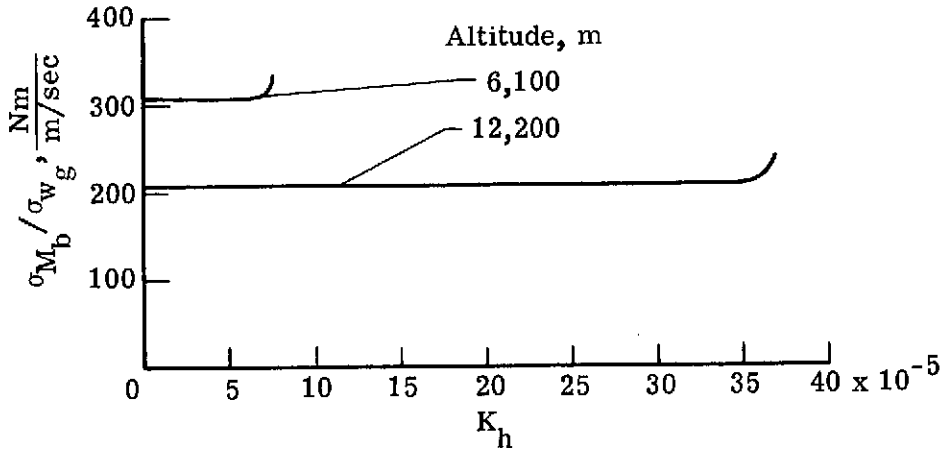

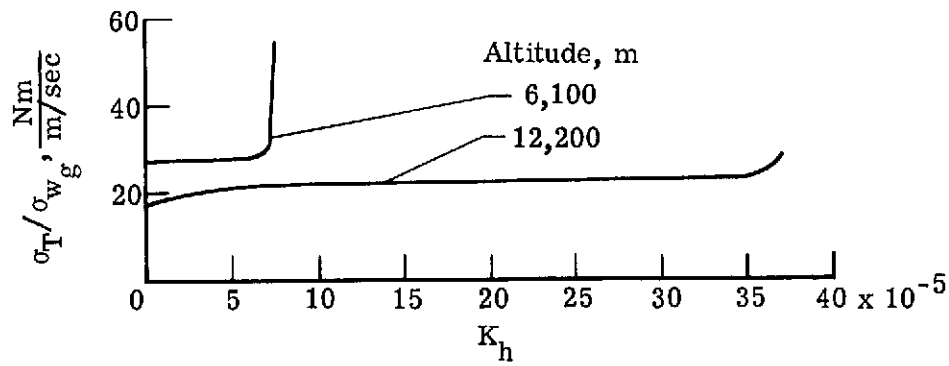

Figure 10.- Concluded.

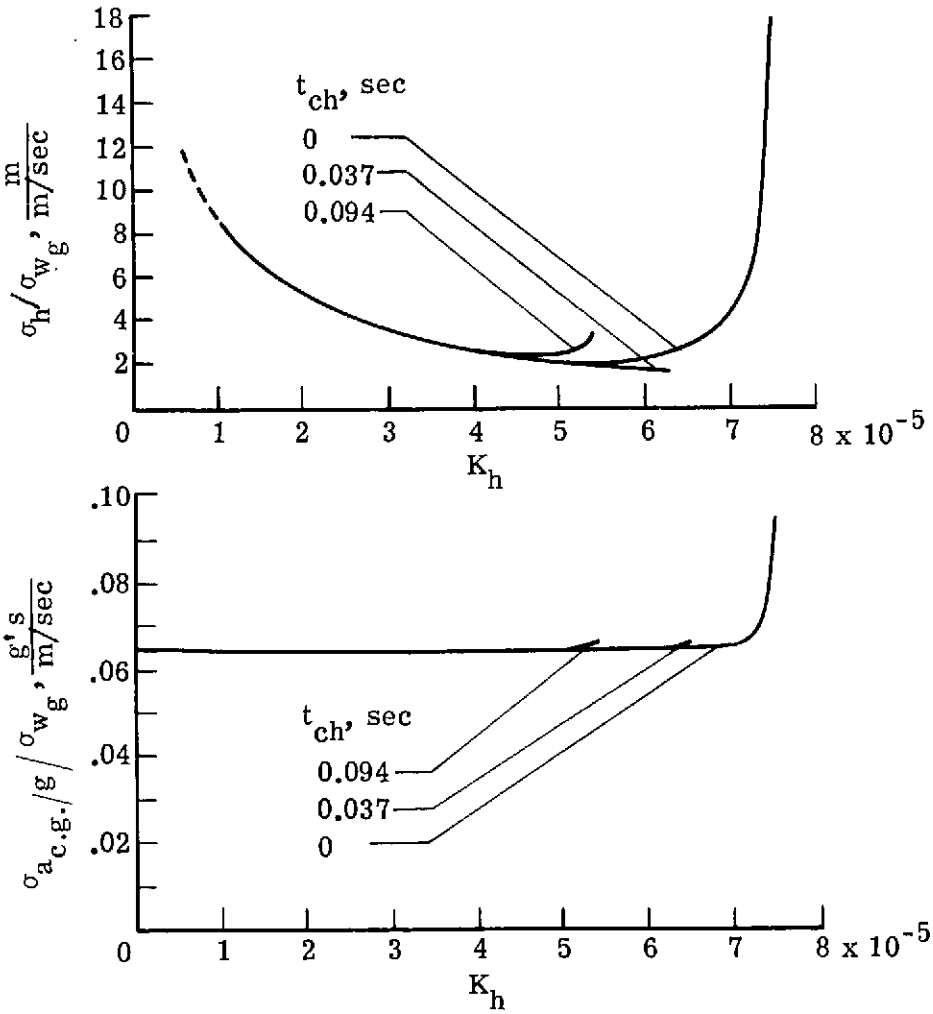

Figure 11.- The effects of altitude-perturbation feedback gain, K_h, on airframe and tail-load responses for three servosystem lag times. Flight conditions I, IV, and V (table II).

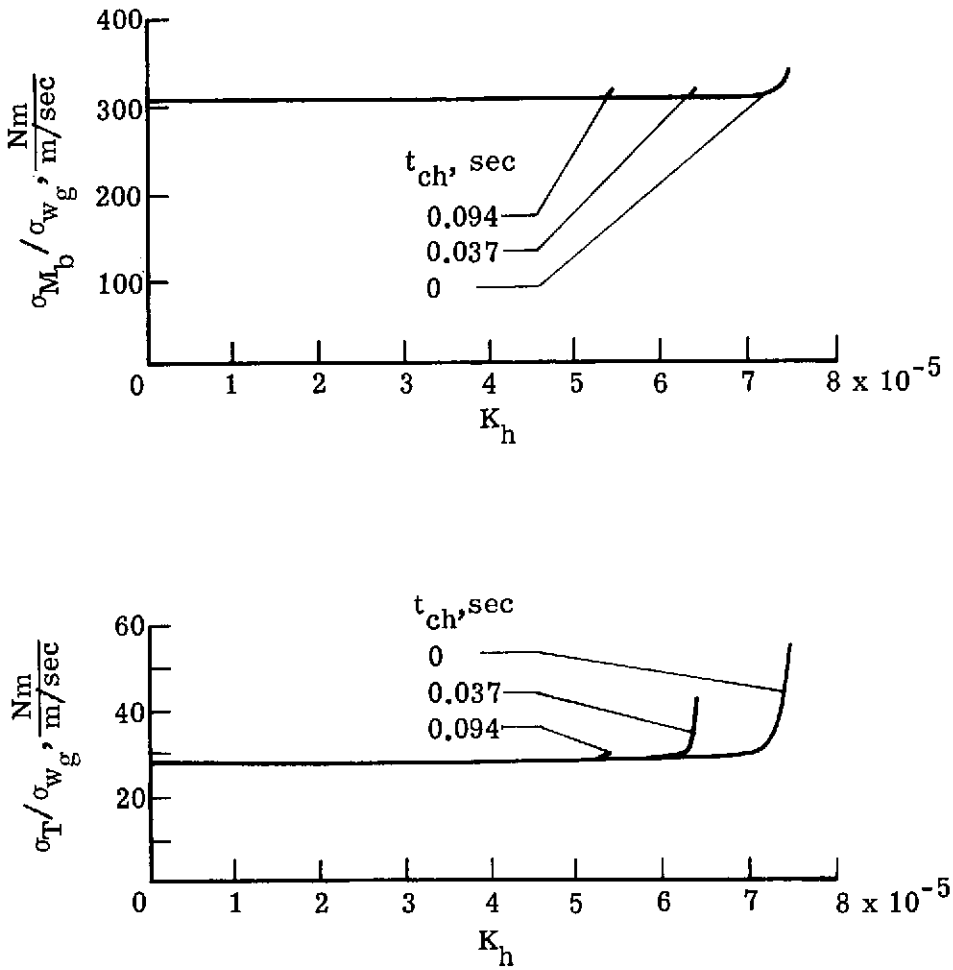

Figure 11.- Concluded.

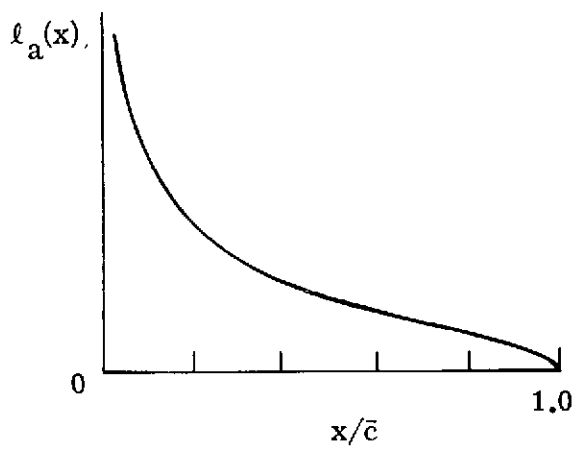

(a) Chordwise "additional" lift distribution for a thin airfoil with a plain trailing-edge control surface.

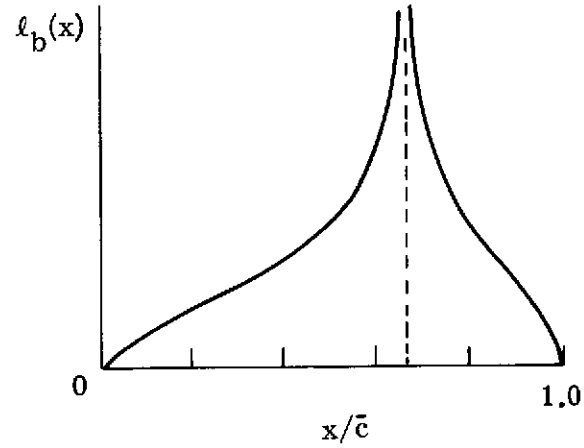

(b) Chordwise "basic" lift distribution for a thin airfoil with a plain trailing-edge control surface.

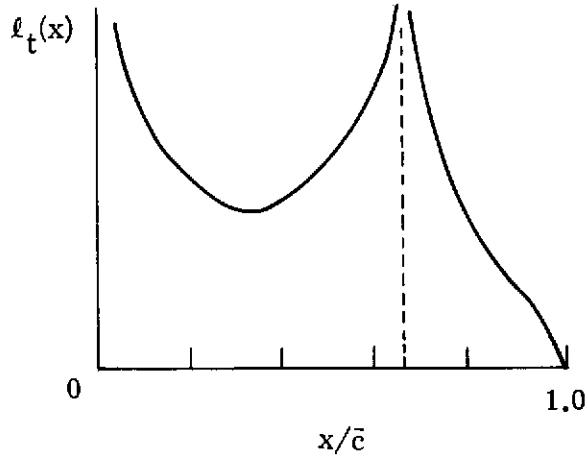

(c) Chordwise lift distribution for a thin airfoil with a plain trailing-edge control surface.

Figure 12.- Chordwise lift distributions.

NASA-Langley, 1973 — 2 L-8756